Image Quality and Dose of an Accelerator-Integrated kV CBCT Systems

by

Amani Shaaer

A thesis submitted
in partial fulfillment of the requirements
for the degree of Master of Science
in Physics

School of Graduate Studies
Laurentian University
Sudbury, Ontario

THESIS DEFENCE COMMITTEE/COMITÉ DE SOUTENANCE DE THÈSE
Laurentian Université/Université Laurentienne
Faculty of Graduate Studies/Faculté des études supérieures

Title of Thesis Titre de la thèse	IMAGE QUALITY AND DOSE OF AN ACCELERATOR-INTEGRATED KV CBCT SYSTEMS
Name of Candidate Nom du candidat	Shaaer, Amani
Degree Diplôme	Master of Science
Department/Program Département/Programme	Physics
Date of Defence Date de la soutenance	August 13, 2014

APPROVED/APPROUVÉ

Thesis Examiners/Examinateurs de thèse:

Dr. Ubi Wichoski
(Supervisor/Directeur(trice) de thèse)

Dr. Konard Leszczynski
(Supervisor/Directeur(trice) de thèse)

Dr. Michael Oliver
(Supervisor/Directeur(trice) de thèse)

Dr. Shuying Wan
(Supervisor/Directeur(trice) de thèse)

Approved for the Faculty of Graduate Studies
Approuvé pour la Faculté des études supérieures
Dr. David Lesbarrères
M. David Lesbarrères
Acting Dean, Faculty of Graduate Studies
Doyen, Faculté des études supérieures

Dr. William Y. Song
(External Examiner/Examinateur externe)

ACCESSIBILITY CLAUSE AND PERMISSION TO USE

Abstract

The ability of an imaging modality to precisely determine patient anatomy and provide reliable information about tumor position is critical in the radiotherapy process. As image-guided radiotherapy (IGRT) becomes more popular in radiation treatment, its overall quality and performance, such as the image quality and amount of dose delivered, need to be assessed. The research described in this dissertation was focused on investigation of the image quality of the planar and cone-beam computed tomography (CBCT) images of two imaging systems commonly used in radiotherapy: Varian On-Board Imager (OBI) and Elekta X-ray Volumetric Imager (XVI). Several imaging quality tests were performed using current clinical imaging protocols provided with both systems and various types of image quality phantoms. CBCT imaging dose of each system was also estimated using standard CT dose index (CTDI) phantoms and several imaging protocols.

Overall, the image quality between the OBI and XVI was fairly consistent with each other with the exception of high contrast resolution and Hounsfield Unit (HU) accuracy. CTDI of OBI was higher than that of XVI which was related to the different designs and imaging protocols between the two systems.

Acknowledgments

First and foremost, I would like to thank Allah Almighty for his guidance and blessings. Without his help and watchfulness, I would not have finished this research and be where I am today.

I would like to gratefully and sincerely thank my research supervisors, Drs. Ubi Wichoski, Konrad Leszczynski, Shuying Wan, and Mike Oliver for their guidance, understanding, and patience. Without their assistance and dedicated involvement in every step throughout the process, this thesis would never have been accomplished. I am truly fortunate to have been able to work with all of you during my studies at Laurentian University.

Many thanks go to the Graduate Program Coordinator, Dr. Jacques Farine, for his support and help throughout my study, and for always greeting my consultations with a smile. I would like to thank you very much for your encouragement and guidance over these past three years.

A special thank you to the physics faculty members Dr. Mohamed Azzouz and Dr. Eduardo Galiano-Riveros , for their advice and support on many occasions. I am glad to have been one of your students. A million thanks to both of you, as you gave me the strength to make my dream come true!

My infinite gratefulness is reserved for my family, whom I am so blessed to have. Without their confidence and prayers, none of this could have happened. Even though we are thousand of miles apart, you were always there whenever I needed

you. Countless thanks to my best friend and husband, Bander, for supporting me and believing in me as I pursued my goal. You were always around at times when I thought that it was impossible to continue. To my sons, Albaraa and Mooyad, I owe both of you lots of fun hours. I could not imagine doing my Master's without you being in my life. To all my friends, thank you for always being there for me whenever I needed a true friend.

Finally, I would like to express my utmost earnest gratitude to our king, Abdullah bin Abdulaziz Al Saud for establishing The King Abdullah Scholarship Program, which sponsored my education. A special thanks to the Saudi Arabian Cultural Bureau in Canada that facilitated everything from my first day in Canada to my graduation.

To each of these individuals, I extend my deepest appreciation.

Contents

Abstrast **iii**

Acknowledgments **iv**

Table of Contents **vi**

List of Figures **ix**

List of Tables **xii**

1 Introduction **1**

2 Background **3**

2.1 Interaction of photons with matter 3

2.1.1 Photoelectric Effect 6

2.1.2 Compton Scattering 6

2.1.3 Pair Production 7

2.2 kV X-ray Production 8

2.3 kV X-ray Detection 10

3 Imaging in Radiation Therapy **12**

3.1 Preface 12

3.2 The Role of Imaging in Radiation Therapy 14

3.3 Image Guided Radiotherapy 17

3.4 IGRT Imaging Techniques 18

3.4.1 Portal Images 18

3.4.2 CT on Rails 19

3.4.3 CBCT Systems in IGRT 20

3.4.4 Helical Tomotherapy 22

3.4.5 Image Registration for IGRT 22

3.5 Quality Assurance for CBCT-based IGRT 24

3.5.1 System Mechanical Safety 24

3.5.2 Geometric Accuracy 25

3.5.3 CBCT Image Quality 26

3.5.4 Registration and Correction Accuracy 26

3.5.5 Dosimetric Measurements 27

3.6 Summary 28

4 Materials and Methods **30**

4.1 The Varian® OBI System 31

4.2 The Elekta® XVI System 34

4.3 Image Quality Tests 37

4.3.1 Planar kV Image 37

4.3.2 CBCT Image 39
4.4 CBCT Dose 43

5 Results **47**

5.1 Image Quality 47
5.1.1 Planar kV Image 47
5.1.2 CBCT Image 48
5.2 CBCT Dose 59
5.2.1 Varian OBI measurements 59
5.2.2 Elekta XVI measurements 61

6 Discussion **63**

6.1 Planar kV image 63
6.2 CBCT image 64
6.3 CBCT dose 69

7 Conclusions **72**

Bibliography **74**

List of Figures

2.2 Regions of predominance of different types of photon interactions with material. 4

2.4 Diagrammatic representation of an X-ray tube used in medical imaging. 9

2.5 The detection method for an indirect detector. An X-ray beam interacts with the scintillator and produces light photons which are detected by an aSi array. 11

3.1 Benign glandular tumor versus malignant glandular tumor. 13

3.2 Kilovoltage imaging modality (1960). 15

3.3 Schematic illustration of the different volumes as defined by the ICRU reports 50 & 62. 16

4.1 The kV CBCT systems used in this study, left: the Varian OBI, right: Elekta XVI.* 31

4.2 Full and half bow-tie filter used in the OBI imaging system. 32

4.3 The OBI system acquisition modes for (a) full-fan mode and (b) half-fan mode. 1- kV source and 2- kV flat-panel detector. 33

4.4 Geometry of the small and large FOVs. 1-kV source reference axis, 2-kV source focal spot, 3-Projection of X-ray field, and 4-kV detector. 35

4.5 Collimator cassettes for small, medium, and large FOVs, (Left to right): S20, M20, and L20. The figure also depicts collimator cassette for medium FOV, label 10 (M10). 36

4.6 The TOR 18FG Leeds phantom (left) and its kV planar image (right). High contrast resolution and low contrast sensitivity modules are located in the central and peripheral region of the phantom, respectively. 38

4.7 (a) Catphan®500, (b) Illustration of CTP 504 model. 39

4.8 The modules of the Catphan phantom (model: CTP 504). 42

4.9 The necessary tools used for measuring CBCT dose. (1) Radcal dose monitor (electrometer), (2) Radcal CTDI ion chamber, and (3) head and body phantoms. 45

5.1 Planar images showing the high contrast resolution for (a) Clinac 4, (b) Clinac 5, (c) Infinity 1, and (d) Infinity 2. The arrow shown in each figure represents the 11th bar pattern. 49

5.2 Planar images showing the low contrast sensitivity. (a) Clinac 4, (b) Clinac 5, (c) Infinity 1, and (d) Infinity 2. The arrow shown in each figure represents the maximum disk reported. 50

5.3 Images of high contrast resolution module using pelvis protocol for (a) Clinac 4, (b) Clinac 5, (c) Infinity 1, and (d) Infinity 2. The arrow shown in each figure represents the maximum lp/cm reported for pelvis protocol. 51

5.4 Images of high contrast resolution module using standard-dose head protocol for (a) Clinac 4, (b) Clinac 5, (c) Infinity 1, and (d) Infinity 2. The arrow shown in each figure represents the maximum lp/cm reported for head protocol. 52

5.5 Images of the low contrast sensitivity module using pelvis protocol for (a) Clinac 4, (b) Clinac 5, (c) Infinity 1 and (d) Infinity 2. 56

List of Tables

4.2.1 The collimator cassette labels and their irradiated length at isocenter. . . 36

4.3.1 The X-ray parameters used in the planar kV images with the Varian OBI and Elekta XVI units. 38

4.3.2 Some of the materials present in CTP 404 module and their nominal CT numbers with comparison to water. 40

4.4.1 Detailed CBCT parameters of the XVI system as well as the $CTDI_w$ values from the XVI reference guide. 45

4.4.2 Detailed CBCT parameters of the Varian OBI system as well as the $CTDI_w$ values from the OBI reference guide. 46

5.1.1 The measured HU values using Varian OBI and Elekta XVI systems for two different imaging protocols. 54

5.1.2 HU values in ROIs in the uniformity module in the Catphan phantom using Varian OBI and Elekta XVI systems, respectively. The maximum HU differences for both types of system are also shown. 58

5.2.1 Measured dose on the CTDI head and body phantoms for various CBCT protocols using Varian OBI system. 60

5.2.2 Measured dose on the CTDI head and body phantoms for various CBCT protocols using Elekta XVI system. 62

Chapter 1

Introduction

The importance of imaging in radiotherapy now goes beyond diagnostic assessment and treatment planning. Recent technical developments in the field of radiotherapy have enabled the integration of imaging techniques into daily delivery of radiation at the linear accelerator. Image-guided radiotherapy (IGRT), where the patient is imaged in the treatment position before, during and/or after the treatment, improves precision and accuracy of treatment delivery.

Several imaging modalities are used for IGRT but none more prevalent than kilovoltage cone beam computed tomography (kV CBCT) system, in which a volumetric image of a patient is reconstructed to evaluate and correct setup uncertainties before the treatment. Since such imaging systems play a vital role in radiotherapy, it is important to investigate their features and limitations as well as to setup a quality assurance (QA) program to ensure accuracy of image quality and dose.

The systems analyzed in this study are the Varian On-Board Imager (OBI) and Elekta X-ray Volumetric Imager (XVI) in the kV planar and CBCT modes. The quality of images and doses were investigated for both systems using different types of phantoms and scanning protocols.

Chapter 2 of this dissertation provides a general overview of basic physics and imaging concepts used in kV imaging, including the interactions that lead to the kV X-ray production as well as a description of kV X-ray detection. Chapter 3 introduces the concept of IGRT, a review of its techniques, image registration methods, and a discussion of CBCT-based IGRT QA program. Chapter 4 presents a description of the Varian OBI and Elekta XVI systems in terms of image acquisition and clinical protocols, testing methods and phantoms used to evaluate images quality and dose measurements. The results of these tests are presented in Chapter 5, while their interpretation is discussed in Chapter 6. Chapter 7 concludes the work.

Chapter 2

Background

The research of this dissertation is aimed at evaluation the quality and dose of kV imaging. The following chapter explains the basic physics of interactions of photon with matter, kV X-ray production and detection.

2.1 Interaction of photons with matter

X-ray imaging, in general, is dependent upon the interactions of a photon beam with matter. When a photon beam is incident on a material, some of the photons will interact, while the rest pass through the material unaffected. At the energy range used in medical imaging, three different types of interactions can occur: photoelectric effect, Compton scattering, and pair production. These interactions are schematically presented in Figure 2.1. The probability of each of these interactions is based on the atomic number Z of the medium and the incident photon energy $h\nu$, where h is Planck's constant and ν is the frequency of the beam, as illustrated in Figure

2.2. The most common interactions involved in the production of kV images are the photoelectric effect and Compton scattering.

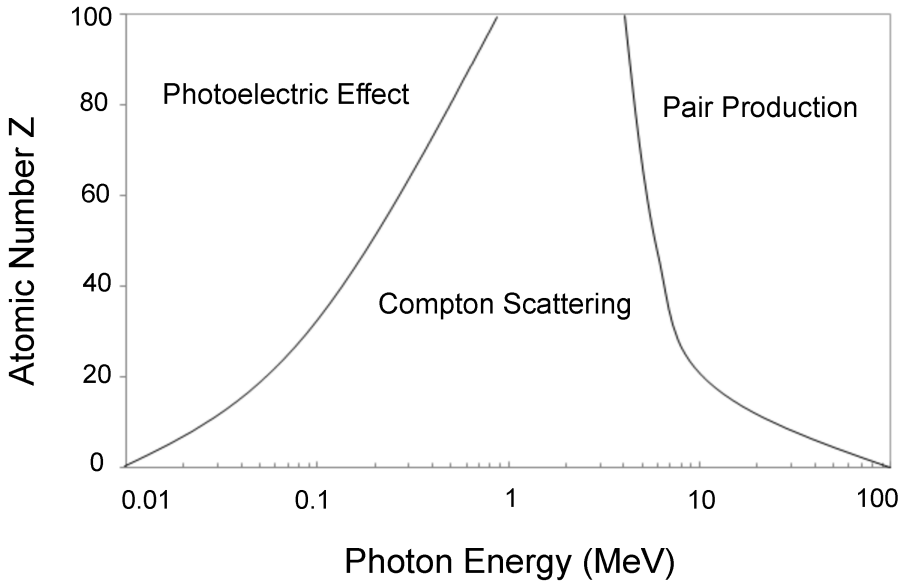

Figure 2.2: Regions of predominance of different types of photon interactions with material.[1]

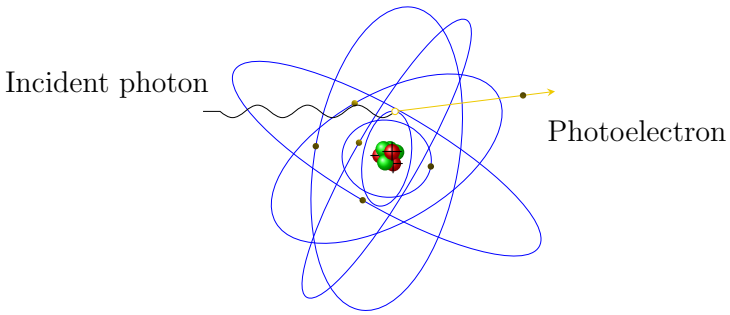

(a) Photoelectric effect

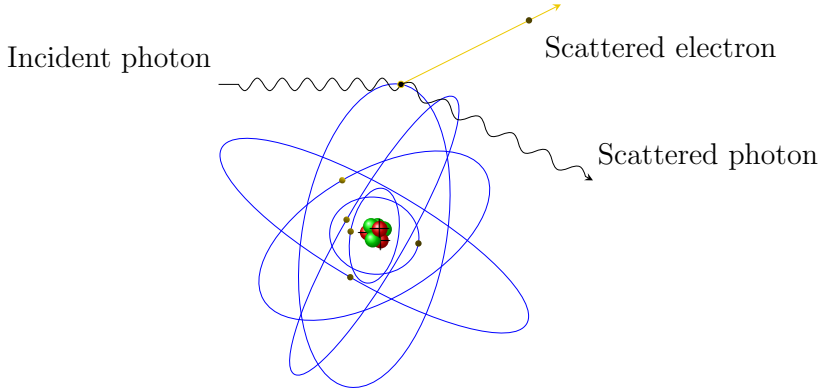

(b) Compton scattering

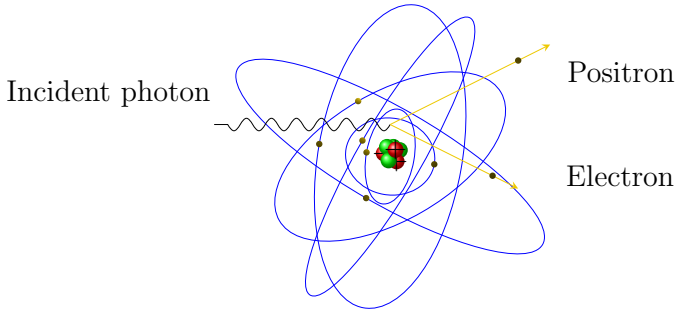

(c) Pair production

Figure 2.1: Interaction of photons with matter.

2.1.1 Photoelectric Effect

The photoelectric effect involves an interaction between a photon and a bound electron, in which the photon is entirely absorbed by the atom and all of its energy ($h\nu$) is transferred to the electron. The electron will be ejected with kinetic energy of $E_k = h\nu - E_B$, where E_B is the binding energy of the electron. The ejection of the orbital electron creates a vacancy in the shell and leaves the atoms in an excited state.[2] The excited atom can return to its ground state by emission of either characteristic X-rays or Auger electrons.

The probability of photoelectric effect is dependent upon the photon energy. If the energy of the photon is less than the binding energy of the electron then a photoelectric effect can not occur. The photoelectric effect is most likely to occur when the photon energy is slightly exceeds the binding energy of the electron. As the photon energy increases further the probability decreases. For this reason, the photoelectric effect is the dominant interaction in medical imaging using kV X-rays. The photoelectric effect also depends upon the atomic number Z. For example, the atomic number of bone is much higher than that of soft tissue, therefore, bone and soft tissue can be easily differentiated in a kV X-ray imaging.

2.1.2 Compton Scattering

The Compton scattering, also known as incoherent scattering , is an interaction between a photon and a free electron. A free electron is defined as an electron whose binding energy is much less than energy of of the photon (i.e. $E_B \ll h\nu$). In this

process, the orbital electron interacts with the incoming photon and is ejected at an angle θ, and a photon of less energy is scattered at an angle ϕ. The kinetic energy of the emitted electron is a function of the energy of the photon, the rest energy of the electron, and the angle of the scattered photon (ϕ), and is given by the following equation:[2]

$$E = h\nu \frac{\alpha(1 - \cos\phi)}{1 + \alpha(1 - \cos\phi)} \tag{2.1}$$

Where $\alpha = \frac{h\nu}{m_0 c^2}$, in which m_0 is the rest mass of the electron, c^2 is the speed of light, and $m_0 c^2$ represents the rest energy of the electron (0.511 MeV). The probability of the Compton scattering increases as the incoming photon energy increases and then starts to decrease as pair production occurs. Compton scattering is independent of atomic number Z, therefore, in an image using MV X-rays, bone and soft tissue are hardly differentiated.

2.1.3 Pair Production

Pair production is the interaction between a photon and the electromagnetic field of a nucleus in which energy is converted into mass. The photon disappears and gives up all its energy to produce a particle-antiparticle pair: electron (e^-) and positron (e^+). In order for pair production to take place, the photon energy must be at least 1.022 MeV because the rest mass energy of each of the electron and positron is 0.511 MeV. The probability of this interaction increases with the atomic number of the material since the pair production process occurs within the Coulomb field of the nucleus. Any photon energy above this threshold energy will be shared between the

particle-antiparticle pair as kinetic energy, namely[3]

$$h\nu - 1.022 = E_- + E_+ \tag{2.2}$$

Here E_- and E_+ are the kinetic energy of the electron and the positron, respectively. The total kinetic energy given to the particles can be distributed between electron and positron in many ways such as one particle receiving all the energy and the other none or most likely each particle receiving half of the total kinetic energy. The energy range in which pair production dominates is 25 MeV and above, and it occurs occasionally in radiotherapy treatment with high energy beams.

2.2 kV X-ray Production

To produce X-rays, electrons must be generated through the use of an X-ray tube. Figure 2.4 represents a schematic illustration of the components of an X-ray tube. The source of electrons in the X-ray tube is the negative electrode or the cathode, which has a tungsten filament that is heated by passing an electric current through it.[2] As the filament is heated, a cloud of electrons will form around the filament. The electrons are then accelerated from the cathode to the anode (positive electrode) by a high potential difference (ΔV) applied across the X-ray tube (20 to 150 kV). The X-rays are then produced via two different processes: Bremsstrahlung and characteristic X-rays processes. Bremsstrahlung production occurs when electrons travel close to a strong electric field caused by the positively charged nuclei of the anode material, causing the decelerated electrons to radiate energy. The decelerated electron will lose a fraction of its energy as a bremsstrahlung X-ray and then continue to interact with

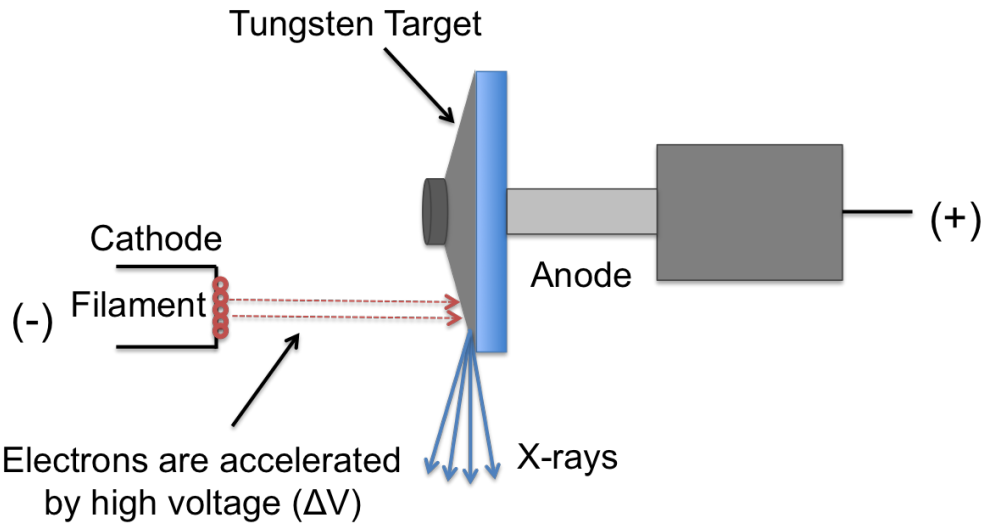

Figure 2.4: Diagrammatic representation of an X-ray tube used in medical imaging.

other atoms in the target material. The characteristic X-ray photons are produced when the incident electron collides with an orbital electron of the anode atoms. In this collision, both electrons are ejected from the target atom leaving a hole in the shell which will be filled by an outer shell electron. As a result, a photon is produced with an energy that is equal to the difference in the binding energies of the two electron shells. The resulting X-ray beam, a cone-shaped beam, can be filtered and reshaped by using different types of filters and collimator.[4]

The number of accelerated electrons per second can be determined by the X-ray tube current (mA), in which 1 mA equals to 6.24×10^{15}electrons/sec.[4] Moreover, the potential difference between the cathode and anode determines the amount of energy gained by these electrons. An electron that is generated by the applied potential of 120 kV will reach the anode with energy equal to 120 keV. The peak voltage (kVp) of the X-ray tube defines the maximum energy that electrons can obtain.

Increasing the tube current as well as the exposure time will result in accelerating a high number of electrons from the cathode to the anode. Thus, the X-ray spectrum can be scaled by the product of the tube current (mA) and the exposure time (s), known as milliampere seconds (mAs).[5] Changing the mAs will alter the number of X-ray photons being produced at a specific energy.

2.3 kV X-ray Detection

The spectra that emerge from an imaged object differ in the X-ray intensity, which is dependent upon the area where they pass through the object. These variations in the intensity are detected to create a radiographic images. Most imaging modalities use standard flat-panel detectors (FPD) that are generally composed of a amorphous silicon (aSi) and a scintillator.

Clinically, an indirect detector system, a scintillator-based X-ray detector, is widely used (Figure 2.5). In this detector, the scintillator converts the energy from the incident X-rays to visible light photons. These photons then strike a silicon photodiode array that generates a potential difference or electrical charge, which is proportional to the intensity of the light. After each exposure of X-ray, the electrical charge is collected and converted (digitized) into a gray scale (pixel value) that is used to represent an image. In other words, these pixel data are an electronic representation of an image of the object.[6]

It should be noted that the intensity of light photons and the produced electrical charge are proportional to the intensity of X-ray photons incident on the surface of

the detector.[6] Moreover, most flat panel detectors use Cesium-Iodide (CsI) as the scintillator since it is considered an excellent absorber of X-ray photons.

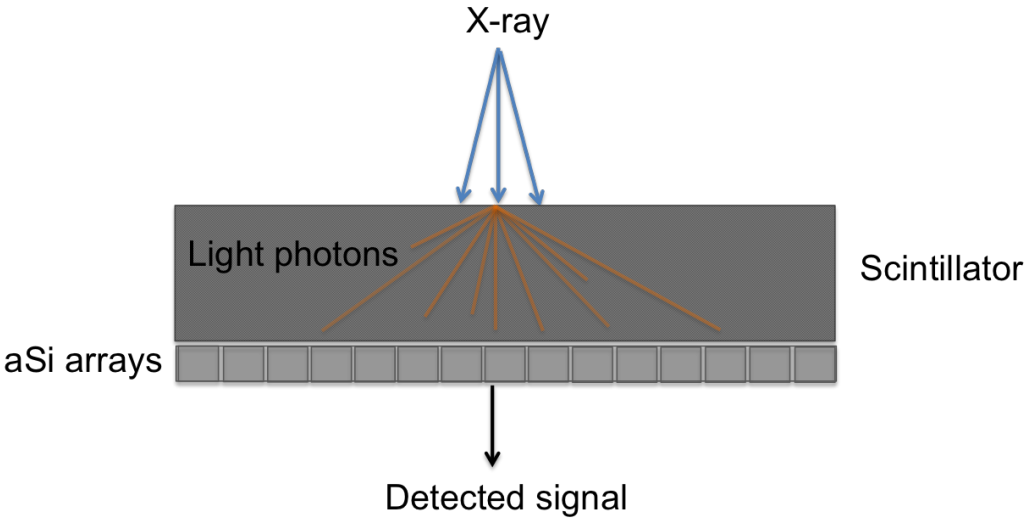

Figure 2.5: The detection method for an indirect detector. An X-ray beam interacts with the scintillator and produces light photons which are detected by an aSi array.

Chapter 3

Imaging in Radiation Therapy

3.1 Preface

Cancer starts when cells in one part of the body begin to grow out of control. Unlike normal cells, cancer cells do not stop growing and reproducing cells. Also, they can invade or grow into other organs or tissues. This process is called metastasis and happens when abnormal cells get into the lymph vessels or bloodstream and form secondary tumors. The term cancer applies only to a malignant tumor, in which abnormal cells destroy nearby tissues. Tumors that are not cancerous are called benign. This kind can grow large but can not invade other tissues, and removing the mass of the tumor usually leads to a complete cure. Most cancer types are named for the part or organ in which they start. Carcinoma, for example, is a malignant cancer originating from epithelial cells, and is considered the most common type of cancer in humans. An example of a benign tumor is adenoma, which is a non-cancerous epithelial tumor with a glandular organization. A malignant version of this type of

cancer is known as drosarcoma or adenocarcinoma (Figure 3.1).[7] As shown in the figure, a benign glandular tumor stays within the basal lamina, which defines the boundary of the normal tissue (duct), while a malignant glandular tumor damages duct integrity.

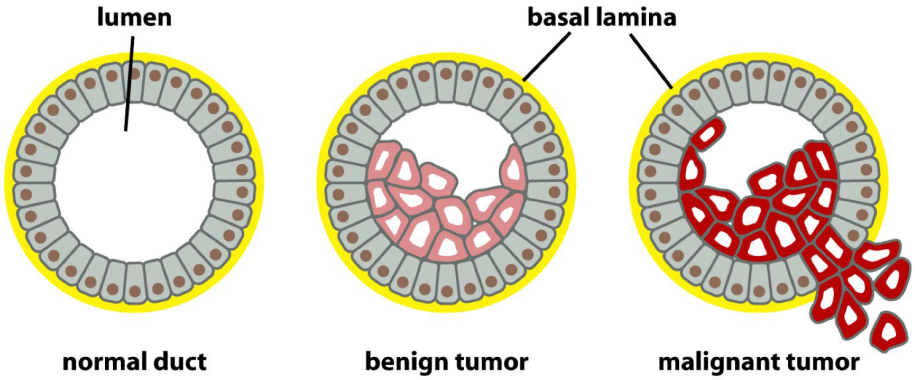

Figure 3.1: Benign glandular tumor versus malignant glandular tumor.[7]

Treatment of cancer depends upon many factors such as type and stage of cancer, the patient's health and preferences, and possible side effects of the treatment option. Surgery, for example, is one option that is used to diagnose, treat, or to prevent recurrence of cancer. It is considered an effective treatment plan if the cancer has not spread to other parts of the body. Furthermore, there is chemotherapy, the use of drugs based on the type of cancer and its stage to destroy cancer cells by stopping them from growing and dividing. Unlike chemotherapy, targeted therapy is a drug used to target the gene alterations in cells that cause cancer with less damage to healthy cells.[8] Radiation therapy is also considered as an effective treatment option for many types of cancer. The main objective of radiation therapy is to deliver a high dose to the target area with minimum dose to surrounding normal tissues. The radiation beam can be delivered to the patients by using an external source of radiation, which

is called external-beam radiation therapy, or by inserting a radioactive material into the body close to cancer cells, known as brachytherapy.[9] The most common type of radiotherapy treatment is the external-beam radiation therapy, such as the use of a linear accelerator to create a megavoltage radiation beam.

3.2 The Role of Imaging in Radiation Therapy

The success of radiotherapy strongly depends upon the accuracy of delivering the desired dose to the tumor volume with minimal dose to normal tissues. This is not an easy task to achieve due to some uncertainties that occur between or during the treatments and this is why most modern radiotherapy modalities are image based. In fact, imaging plays an important role in each step of the radiation therapy process beginning at diagnosis and continuing through treatment planning, delivery, and treatment follow up. In the early stage of image guidance in radiation therapy, both megavoltage (MV) and kilovoltage (KV) portal imaging were used to align the patient with the treatment beam (Figure 3.2).[10] The use of portal images was not enough to visualize target volumes and it limited the images and the treatment planning to two dimensions.

In the 1970's, the invention of the computed tomography (CT) made it possible for oncologists to visualize a three dimensional image of any part of the body in a non invasive way. Anatomical information on CT images are presented in transverse slices based on electron density with high contrast resolution and excellent soft tissue contrast.[11]

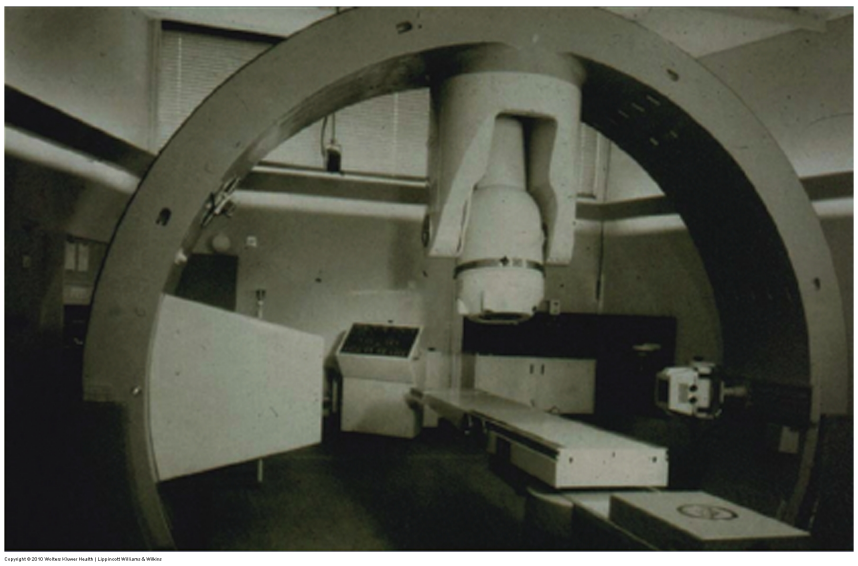

Figure 3.2: Kilovoltage imaging modality (1960).[10]

Modern treatment delivery is dependent on kV CT images to accurately position the patient on the treatment table. The position of the patient is usually checked with skin markers and/or bony structures. However, this positioning technique may involve some uncertainties since the internal patient anatomy changes with time; this kind of movement is known as interfractional motion. For instance, the shape and position of the prostate are significantly dependent on the filling of the rectum and the bladder. Furthermore, the motion of the prostate is independent of the bony structures; thus its position can not be precisely established by bony landmark registration. Intrafractional motion is another type of motion that leads to geometric uncertainties. It is the motion of the anatomy during the treatment session such as respiratory motion or cardiac motion. As a matter of fact, those geometrical uncertainties can be reduced in different ways; however, they can not be totally eliminated.

Advances in current imaging modalities have greatly elevated the resolution and contrast of the patient anatomy. Practically, the basic tumor target volume, known as gross tumor volume (GTV), is obtained from a conjunction of different imaging modalities (CT, MRI, PET, ultrasound, etc,) as well as clinical examination.[11] The gross tumor volume as defined in the ICRU report 50 is "...the gross palpable or visible demonstrable extent and location of malignant growth".[12] In order to cover all microscopic disease surrounding the visible target and other areas at risk the GTV is expanded to establish the clinical target volume (CTV). The CTV is either a fixed or variable margin around the target volume (e.g. CTV = GTV + 1 cm).[11] To account for the internal motion of organs contained in or adjacent to the CTV, the internal target volume (ITV) is added.[13] Around the ITV expansion is a planning target volume (PTV). This volume is designed to account for setup uncertainties. The larger the variability of the motion and setup, the larger should be the PTV. Schematic representation of the volumes of interest is shown in Figure 3.3.

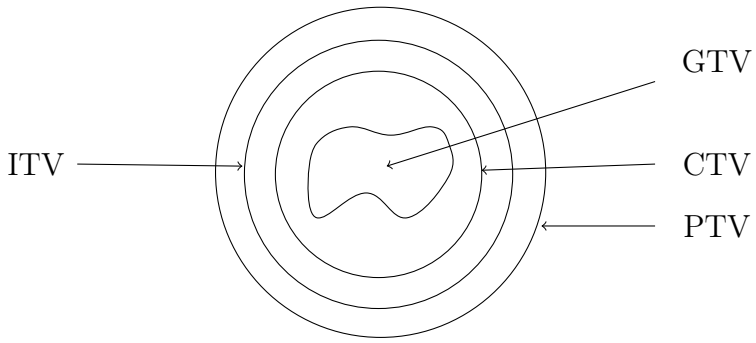

Figure 3.3: Schematic illustration of the different volumes as defined by the ICRU reports 50 & 62.[12,13]

The unfortunate consequence of adding these margins is that it limits the target dose escalation due to dose limits on nearby organs at risk. Exposing normal tissues within margins to a high dose may cause unacceptable morbidity. Therefore, it is useful to reduce the margin size while keeping the target irradiated. Nevertheless, reducing the margin size can lead to a significant problem if the patient anatomy and position are not accurate or different from the treatment plan. This will result in motion blurring of the dose within tumor volume.[14] Required accuracy of dose distribution in the target and patient position require proper use of image guidance techniques during radiotherapy.

3.3 Image Guided Radiotherapy

Imaging has a wide application in radiotherapy, therefore different definitions of image-guided radiation therapy (IGRT) have been used. It involves imaging the patient within the treatment room before irradiation to ensure accurate treatment.[15] IGRT is defined as the use of on-board imaging prior to treatment to guide patient position and set up. In fact, it is difficult to administer a relatively high dose to the planned target without uncertainties, such as patient set-up and anatomy motion. The precise location of the target and adjacent healthy tissues are frequently not known exactly, the use of a safety margin as mentioned earlier is important in this case.

The significant role of IGRT is to target tumors more accurately, and to reduce the exposure to normal tissues during treatment. In addition, IGRT increases the

amount of information collected through the course of the radiation treatment. This information allows the ongoing assessment of the treatment planning techniques such as target margin expansion or shrinkage and the changes of the target size due to radiotherapy. IGRT also enables new planning and delivery techniques that incorporate the information obtained from imaging systems, known as adaptive radiation therapy (ART).[10,16] Adaptive radiotherapy (ART) is defined as the continued use of imaging to monitor the target changes between treatment fractions, in which the tumor changes during treatment is examined prior to every delivery. Thus, the treatment plan can be adjusted to match the deformation of the target.[10] The ART benefit can only be reached if total deformations and records of the target are registered for each radiotherapy fraction, known as image-guided adaptive radiation therapy (IGART).

3.4 IGRT Imaging Techniques

In IGRT, there are many types of imaging modalities that can be used to verify patient position and set up. In this section, we briefly discuss the image acquisition of the most popular IGRT technologies as well as the image registration process in IGRT.

3.4.1 Portal Images

Electronic portal imaging devices (EPID) has been used for decades to verify the patient set-up and position efficiency. The major advantage of the EPID is the production of a digital image of the beam exiting the target with good contrast and

resolution.[14] It is the most widespread on-board IGRT system, first described by Leong et al.[17] Generally, EPID is used to increase the accuracy of the alignment between the treatment beam and target. In addition, the EPID can be used for quality assurance and dose verification before the beginning of radiation treatment.[18] A megavoltage (MV) electronic portal imaging device, for example, can verify the accuracy of patient position as well as monitor target position during a treatment session.[2,16] There are two main limitations of this technology: the first it can not provide a three-dimensional volumetric image of the target; the second it has insufficient low contrast sensitivity of patients' anatomy at MV energies due to the dominance of the Compton effect.

3.4.2 CT on Rails

Volumetric imaging and in particular CT provides an accurate geometric data of the target and its surrounding normal tissues. Most volumetric IGRT imaging techniques give a static image of the target such as tumor position. Such techniques are able to assess whether the planning target volume (PTV) margin precisely covers the target area.[19] The first example of volumetric imaging is in-room CT scanners, in which a separate CT scanner is housed over the treatment table using special rails. To acquire a pre-treatment CT image, the treatment couch is moved to be aligned with the CT scanner. The latter is then rotated in the axial orientation relative to the patient. At the end of the process, the treatment table is moved back into alignment with the linear accelerator gantry. The main benefit of the in-room CT system is providing

a high-quality three-dimensional image of patient anatomy, which is important to localize the tumor and to reconstruct dose distribution within the target.[10]

3.4.3 CBCT Systems in IGRT

Cone beam CT imaging technique is the most recent advancement in volumetric imaging IGRT. Nowadays, cone beam computed tomography (CBCT) is used with a diagnostic X-ray tube and a large-area flat panel detector to test the accuracy of patient position during radiation therapy. Using CBCT prior to treatment session, a full CT scan of the patient is acquired in less than 2 minutes. Following that, the CT scan is registered to a reference CT data to facilitate accurate positioning of the patient to the treatment beam isocenter.[20] The CBCT image that is created looks similar to a three-dimensional fan beam CT image; however, the image quality is not as good as FBCT.[21] A fan shaped X-ray beam is a traditional CT scan that obtains an image by acquiring one or more thin slices per rotation, in which the length of the slice is between 0.06 and 2.4 cm.[22] CBCT image quality is limited compared to the FBCT due to the scattered radiation produced by a volumetric image acquisition. The two most popular CBCT systems are briefly discussed in the following subsections.

Kilovoltage CBCT

Kilovoltage CBCT is the most common application of three-dimensional cone-beam CT. It is based on tomographic images obtained at the time of radiation therapy. Besides tomographic imaging kV CBCT is also capable of producing radiographic and fluoroscopic images from the same X-ray source and detector. In kV CBCT, the

X-ray tube is positioned at 90° relative to the central axis of the linear accelerator beam. To acquire an image, an amorphous silicon (aSi) flat-panel detector is mounted opposite to the X-ray tube to detect the kV X-rays beam. The gantry rotates 180° or more to obtain planar projection images from different directions.[2] The reconstructed volumetric images show good low contrast tissues, which is useful in determining the gross volume of the target (GTV). The goal of IGRT is to correct for the displacement of the target relative to its planned position. Using daily IGRT with kV CBCT has proven that it is possible to reduce the PTV margin to up to 50% for head and neck cancer patients.[23] Such a reduction in the PTV margin leads to reduction in radiation toxicity with equivalent local target control. Unlike MV beam, the kV beam deposits much higher doses in bones than in soft tissues. This is attributed to the fact that the photoelectric interactions are highly dependent upon the atomic number Z.

Megavoltage CBCT

Similar to kV CBCT, megavoltage CBCT is used to acquire a volumetric image of patient anatomy. Currently, in this approach, EPID employs flat-panel detectors. In addition, the X-ray source used for imaging is the megavoltage radiation beam of the linear accelerator. The benefits of the megavoltage beam are the reduction of scattering and beam hardening artifacts as well as elimination of high Z materials artifacts.[22] To obtain multiple planar projection images, the X-ray source and the detector rotate around the patient at different angles. Although the soft tissue contrast images is much weaker in MV CBCT due to the dominance of the Compton effect at MV energies, the overall quality of the volumetric images is generally useful

for localization of the target.

3.4.4 Helical Tomotherapy

Helical tomotherapy is an integrated-accelerator imager that can be used to acquire fan-beam MV CT images of patient anatomy and deliver sophisticated intensity-modulated radiation therapy (IMRT) treatments. They are called MV CT images since the imaging beam is created by the same linear accelerator that produced the treatment beam. Such property makes tomotherapy a distinct device with the ability of providing IMRT and IGRT using the same treatment apparatus.[2] The accelerator in this technology rotates in a full circle, and at the same time the treatment couch is moving gradually through a donut-shaped accelerator gantry housing also the detector to create a helical motion of the radiotherapy beam with respect to the patient. Unlike CT images, the noise of MV CT images is high with poor soft tissue contrast; however, they have sufficient contrast for patient localization at time of treatment.[24]

3.4.5 Image Registration for IGRT

Image registration is an important step in image guided radiotherapy. The main goal of this process is to correlate different image sets to find corresponding landmarks or regions. In IGRT, the image registration compares the daily IGRT image and the reference image in order to obtain the corresponding adjustments to accurately align the tumor volume to the radiotherapy beam. The reference image is acquired at the time of radiation treatment planning and represents the intended precise alignment

of tumor volume and treatment beam. For example, the reconstructed MV CBCT or kV CBCT images are integrated with the pre-treatment CT images using special image registration software, in which the pre-treatment images are displayed in different colors. For CT on rails, the images in registration process are viewed parallel to each other on the computer screen and can be displayed in different planes such as transverse, sagittal, and coronal planes.[2,25] According to the registration results, the required adjustments to the treatment couch and hence the patient position are automatically performed before the start of radiotherapy.

In most image modalities, the image registration can be achieved manually or automatically. For manual or visual registration mode, the two image sets are superimposed in a way that they can align visually based to anatomical features. In the automatic mode of registration, reference points, curve-like features, or pixel value information are used in both image sets to bring them into alignment. There are two main categories of automatic registration: rigid body registration and deformable registration. In the rigid body registration, the anatomical sites or regions are considered to be rigidly related. The rigid body registration involves rigid transformations between the treatment and reference images, including translations and rotations in 3D coordinate system.

In the deformable registration, there is more freedom in terms of rotations and translations to register the deformation between target and reference images.[10,19] Generally, automatic registration is more accurate and efficient than manual registration. In addition, these IGRT registration modes are slightly affected by the following factors: imaging modality settings such as image quality (e.g. spatial resolution, con-

trast, and noise), anatomical site, and the accuracy of the registration algorithm.

3.5 Quality Assurance for CBCT-based IGRT

Effort spent on quality assurance (QA) of imaging devices in radiology have been dramatically increasing since modern radiotherapy relies on imaging in all stages of patient care. The goal of a QA program is to make sure that the imaging system performance characteristics do not differ from the established baseline at the time of commissioning.[26] The introduction of different imaging modalities and image guidance strategies in radiotherapy, such as the cone beam CT based IGRT, requires appropriate quality assurance and controls. The American Association of Physics in Medicine, AAPM report No 179 contains QA aspects (tests and tolerance) for most CT-based IGRT systems.[22] In general, the commissioning and acceptance procedure includes five aspects of QA: system mechanical safety, geometric accuracy, image quality, registration and correction accuracy, and dosimetric measurements. Each of these tests will be covered in the following subsections.

3.5.1 System Mechanical Safety

Testing the safety and the functionality of the imaging systems is performed on a daily basis and should match the acceptance test procedure provided by the vendor. The initial safety tests should include a functionality check of all system interlocks such as the door interlock, kV or MV source interlock, emergency-off interlock, and touch guards (e.g. kV and MV imaging flat panel arms and linear accelerator head).

It is important to check the door interlock to prevent irradiation when the door of the treatment room is open. The door interlock and imaging system source interlock tests are done by opening the door of the treatment room while the radiation beam is being emitted and when the imaging source arms are not entirely opened.

The aim of testing the emergency stop switch is to protect patients and personnel from equipment collisions and undesirable irradiation by stopping the treatment beam and all motions. The AAPM report No 142 recommends that the safety tests of kV CBCT or MV CBCT should be performed on a daily basis for IGRT application.[26]

3.5.2 Geometric Accuracy

Since the kV imaging system is used to position the patient with respect to the MV treatment beam, it is important to align the isocenter of kV imaging system with the isocenter of the MV treatment system. The latter refers to the point where the center of the MV beam intersects the axis of rotation of the gantry, couch, and collimator. The agreement of kV and MV beam isocenters is tested by aligning the center of a high-contrast object, such as a ball bearing phantom with a diameter of 8mm, with the treatment room laser lines. The laser lines define the vertical and horizontal coordinate planes and point to the MV isocenter. More details on how the measurement is done are provided in the literature.[20,22,26,27] This QA parameter is important for accurate treatment delivery, therefore, a daily test of the geometric calibration should be done to monitor agreement of the isocenters.

3.5.3 CBCT Image Quality

The image quality of kV and MV CBCT imaging systems is significantly influenced by the characteristics of these technologies such as pixel and focal spot size and the geometry of the cone beam. For instance, the large cone beam angle used in CBCT systems leads to an increase of scattering signals on projection images used in reconstruction. The contribution of scatter to the CBCT images decreases the contrast of soft tissue and the accuracy of CT numbers as well as increasing image noise. In addition, since the image acquisition time in CBCT technologies is quite long (≈1-2 mins), the image quality will be affected by the blurring of intrafractional motion. Therefore, on the CBCT-based IGRT systems, it is recommended that measurements of image quality are performed on a monthly or semiannual basis to detect any changes of the system.[22] Image quality tests are performed using special phantoms that consist of different cylindrical sections to test different features of image quality. For example, CatPhan phantom (The Phantom Laboratory, Salem, NY) is used for kV CBCT imaging quality purposes including high contrast resolution, Hounsfield Unit (HU) accuracy, spatial linearity, low contrast sensitivity, and field uniformity.[20] A single scan of this phantom gives a number of quality assurance parameters in a short amount of time.

3.5.4 Registration and Correction Accuracy

As mentioned in section 3.4.5, it is important for imaging system to precisely register a target localization geometry with a reference geometry. In this QA procedure the

registration and couch shift accuracy is tested using different methods and phantoms. On the Elekta XVI system, Lehmann et al. and his group used an anthropomorphic phantom (Rando phantom) to test the algorithm for (re)positioning the patient relative to the isocenter of the treatment beam.[20] This test was performed to accurately detect any shift or misalignment in the position and to determine the precise shift back to the correct position. The phantom was moved in different directions (right, up, and in) relative to the reference position, in which each movement of the phantom was determined by the couch digital readout (1 mm resolution). After detecting these movements, the phantom was repositioned to its initial location relative to the isocenter and a new image was taken. Comparing the resulting image with the reference image showed that the position correction algorithm precisely detected the translational and rotational movements of the phantom with accuracy of 1 mm and 0.6 degree, respectively.

3.5.5 Dosimetric Measurements

Measurement of the dose to patients in CBCT systems is an important quality assurance test in IGRT. It is used to establish the baseline measure of patient dose and to monitor that measure over time. Since the dose distribution across the patient may differ, dosimetry test efficiency in CBCT depends upon the scanning system parameters and techniques. In the past decade, a number of publications have examined the CBCT imaging systems dose delivered to patients. Two main methods have been established to measure the dose in the patient: either by using the Monte Carlo (MC)

code to estimate the dose through simulation in software[28] or by measuring the dose experimentally using special phantoms.[29–34]

Some of these studies used two types of CBCT systems; the Varian OBI (version 1.3/1.4) and Elekta XVI. The measured CBCT imaging doses using these two systems are not identical due to the differences between them in terms of the image acquisition mode, imager filters, detector design, reconstruction techniques, and other factors. In addition, some studies have proven that the dose may be affected by differences in patient size.[30,35–37] Moreover, even when using the same imaging system and phantoms, the concomitant dose may change. Palm et al., made a comparison between two different versions of Varian OBI system software; version 1.3 and 1.4. They found that the imaging dose in Varian OBI v1.4 system is lower than in v1.3.[38] As mentioned above, dose measurement depends upon a number of factors that need to be considered if the large scale application of CBCT-based IGRT technology is to be optimized.

3.6 Summary

In this chapter a general background of radiation therapy and the role of imaging in radiotherapy have been introduced followed by an introduction to image guided radiation therapy (IGRT). Furthermore, the need for accurate methods of quality assurance used to check the system mechanical safety, geometric uncertainties, image quality, registration and correction accuracy, and dosimetric measurements in IGRT technology has been investigated. While CBCT-based IGRT imaging systems have

been used to reduce patient set-up uncertainties, there are a number of quality assurance issues that need to be considered to benefit from the full potential of an on-board imaging technology. These issues include the quality of on-board CBCT images, performance of the CBCT imaging systems, and the quality of the system with respect to patient dose. It is important, therefore, to investigate each of these issues to improve the application of CBCT imaging devices during image-guided radiation therapy.

Chapter 4

Materials and Methods

As mentioned in the previous chapter, the use of imaging devices for verification and correction of patient position prior to treatment has spread widely in the last few years and is known as Image Guided Radiotherapy (IGRT). kV CBCT is a premiere device for IGRT technology with the ability of producing high quality images of the patient. Two kV CBCT systems were investigated in this study: the On-Board Imager (OBI) by Varian and X-Ray Volumetric Imager (XVI) by Elekta (Figure 4.1). This chapter describes those two systems in terms of configurations and scanning protocols. In addition, the various testing methods and phantoms needed for a comprehensive quality assurance of both systems will be covered.

It should be noted that both systems were accepted and commissioned prior to use for treatment and before this study was performed. The image quality and dose assessments were also performed to make sure these imaging systems were consistent over time with the established baseline data.

Figure 4.1: The kV CBCT systems used in this study, left: the Varian OBI, right: Elekta XVI.*

4.1 The Varian® OBI System

In this study, two different units of the Varian OBI were used: one was installed in 2009 (Clinac 5) and the other was installed in 2011 (Clinac 4). The OBI consists of two mounted arms (Exact^{TM}): one for the kV X-ray source (kVS) and the other for the flat panel aSi detector (kVD). Both are mounted on the linac linear accelerator orthogonally with respect to the treatment beam. The kVS X-ray tube has a tungsten/rhenium (W-Re) target angled at 14° and two possible focal spots: small (0.4mm) and large (0.8mm). This X-ray tube generates photon spectra with kVp ranging from 40 to 125 kV.[39] In addition, the kVS has adjustable blades that collimates the X-ray beam (2×2 to 50×50 cm^2 projected at 100 cm from the focal spot). The amorphous silicon flat panel detector has a size of approximately 40×30

*All figures were taken by author unless otherwise indicated.

cm^2.[40] The isocenter of the CBCT imager is at 100 cm from the kVS and the source to detector distance (SDD) can be 140, 150, or 170 cm.[39]

Two types of filters are used to improve CBCT image quality: the full and half bow-tie filters (Figure 4.2). The bow-tie filters are made of aluminum and mounted to the kVS when in use. The main functions of the filters are to reduce X-ray scatter, reduce skin dose, reduce the dynamic range demands on the kVD, and to allow higher energy X-rays to be used without saturating the detector.[40] The full bow-tie filter is used for small anatomical sites such as head and neck while the half bow-tie filter is used for large anatomical regions such as chest, abdomen, and pelvis.

Figure 4.2: Full and half bow-tie filter used in the OBI imaging system.

The kV CBCT image acquisition has two scanning modes depending on the dimension of the anatomical site: full-fan and half-fan modes. If the reconstructed volume diameter is $\leq$25 cm, a full-fan mode is used, in which the center of the kVD is aligned with kVS. For a head protocol, a small field of view (FOV) setting, full-fan mode and full bow-tie filter are used. A total of 350 projections during the 200° gantry rotation are acquired.[41] If the diameter of the reconstructed volume is >25

cm, the CBCT image acquisition is switched to a half-fan mode, in which the kVD is offset laterally by∼15 cm and only half of the scanned object is viewed in each projection. The half-fan acquisition mode with the half bow-tie filter is usually used for body scans such as pelvis and chest with a large FOV setting (45 cm). In this mode, a total of approximately 650 to 700 projections during 360° gantry rotation are obtained. A representation of each scan mode is shown in Figure 4.3.

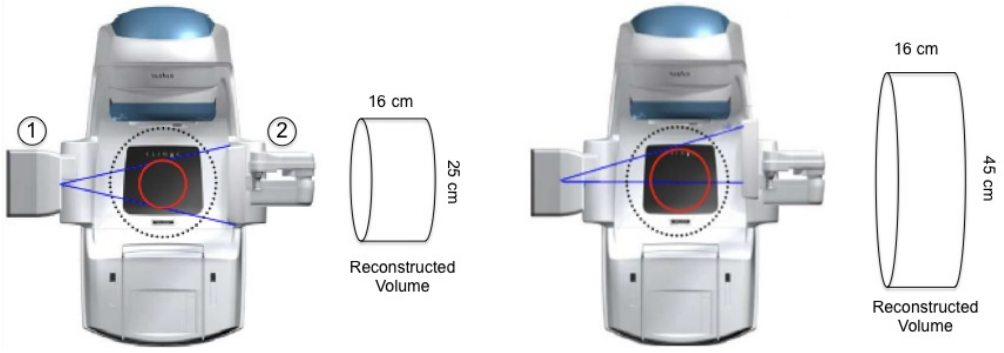

(a) Full-fan mode. (b) Half-fan mode.

Figure 4.3: The OBI system acquisition modes for (a) full-fan mode and (b) half-fan mode. 1- kV source and 2- kV flat-panel detector.[40]

The X-ray parameters, such as tube voltage (kVp), current (mA), and exposure time per projection (ms) are preset for anatomical sites within the OBI software. These techniques depend upon the anatomical site and can be adjusted for each patient.[41]

4.2 The Elekta® XVI System

The other IGRT imager technology that was used in this study is the Elekta Infinity™ X-ray Volumetric Imager (XVI). In this study two different units of Elekta XVI were used: Infinity 1 (installed in 2013) and Infinity 2 (installed in 2014). The kV imaging system consists of kV X-ray source (kVS) with an amorphous Silicon (aSi) flat panel detector (41×41 cm^2) (kVD) mounted orthogonally to the treatment beam. The X-ray tube of the XVI system is capable of maintaining a tube voltage range from 70 to 150 kV and it is positioned at 100 cm from the gantry isocenter. For CBCT image acquisition, the gantry is rotated around the object and images are taken continuously.[20,42]

There are three FOVs in the XVI system: small (S), medium (M), and large (L). In the small FOV setting, the center of the kVD is aligned with the central axis of kVS with X-ray field of diameter of 27 cm (Figure 4.4a). Known as full-fan mode, this setting requires a gantry rotation of 200° to complete the acquisition. It is preferable to use the small FOV mode when scanning head and neck or other anatomical sites of less than 27 cm in diameter. For the medium (41 cm) or large (50 cm) FOV setting, the kVD is shifted laterally by 115 mm or 190 mm, respectively, so that an increase in FOV can be achieved. Both settings require gantry rotation of 360° to complete the image acquisition, known as half-fan mode. A schematic representations of a small and a large FOV are shown in Figure 4.4.

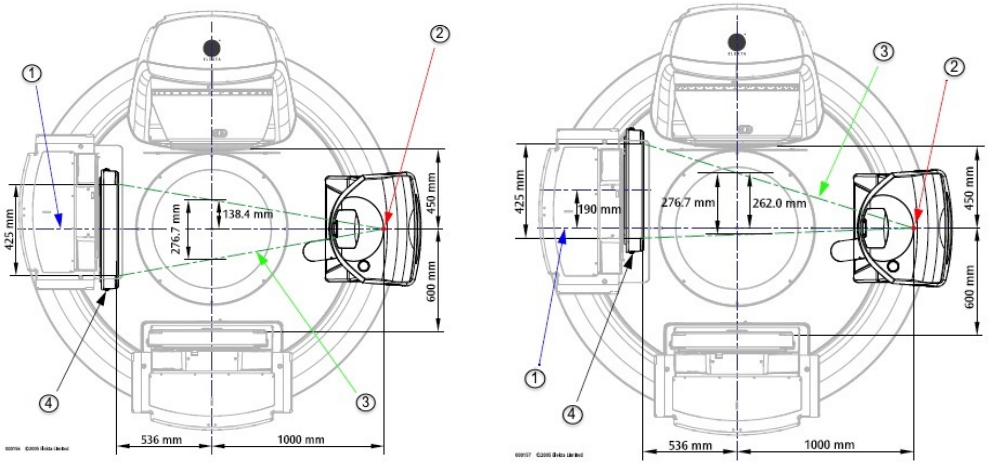

(a) Small FOV (b) Large FOV

Figure 4.4: Geometry of the small and large FOVs. 1-kV source reference axis, 2-kV source focal spot, 3-Projection of X-ray field, and 4-kV detector.[43]

To define the dimension of the X-ray beam, a lead collimator cassette is inserted in front of the X-ray source. Various sizes are available as shown in Figure 4.5. Each cassette has a specific label (2, 10, 15, and 20) that identifies the longitudinal field size.[32,43] Table 4.2.1 lists the cassette labels and their corresponding FOVs and irradiated lengths at the isocenter.[43] Changing the cassette is useful to reduce dose to the patient as well as to reduce scatter that affects the image quality.

Similar to the Varian OBI system, the XVI system has two types of filters: F1 (bow-tie shaped) and F0 (an empty insert). The F1 filter is used for all treatment anatomy sites except for head and neck region, where F0 is preferably used.[44,45] In practice, there are four preset scanning protocols for the XVI system: head and neck, pelvis, prostate, and chest. Each protocol has preset parameters, such as collimator

cassette, kVp, mA, ms, and gantry rotation angles, that are created and stored in the XVI software for clinical use.

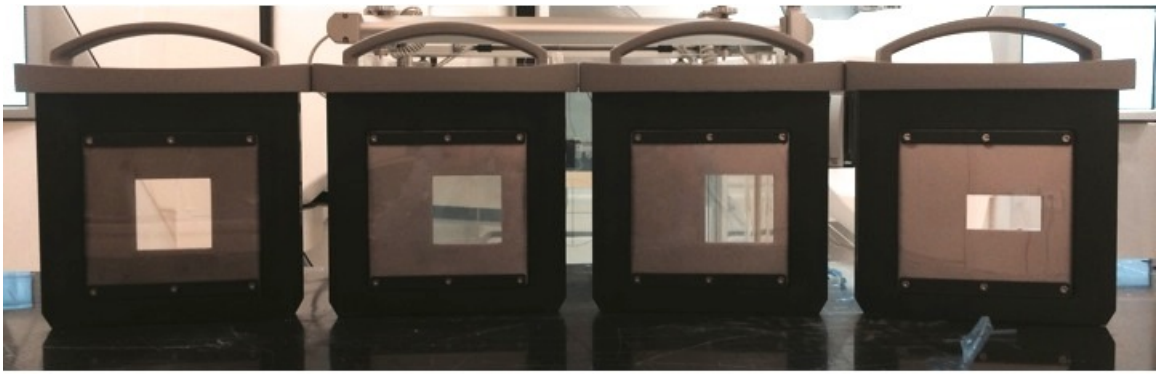

Figure 4.5: Collimator cassettes for small, medium, and large FOVs, (Left to right): S20, M20, and L20. The figure also depicts collimator cassette for medium FOV, label 10 (M10).

Table 4.2.1: The collimator cassette labels and their irradiated length at isocenter.[43]

Label	Irradiated length at isocenter (cm)	Corresponding FOV
2	3.52	Medium FOV
	3.65	Large FOV
10	13.54	Small & Medium FOVs
	14.32	Large FOV
20	27.67	All FOVs
15	17.85	Medium FOV

4.3 Image Quality Tests

Image quality tests were performed to evaluate the quality of planar kV images and CBCT images. These measurements are important to establish baselines in imaging performance as well as to verify consistency in images quality.

4.3.1 Planar kV Image

The two dimensional imaging technique (2D) involves acquisition of a planar radiological images in which the position of the kVS and kVD are fixed. The 2D image quality tests, such as low contrast sensitivity and high contrast resolution, were performed using a TOR 18FG Leeds phantom (Leeds Test Objects Ltd, North Yorkshire, UK), as shown in Figure 4.6. The phantom has 18 disks each 8 mm in diameter and contrast level ranging from 0.81% to 14.9% to evaluate image contrast sensitivity. Moreover, it has 21 bar patterns with spatial resolution ranging from 0.5 to 5 line pairs per millimeter (lp/mm) to evaluate spatial resolution of an image. During the measurements, either with Varian OBI or with Elekta XVI, the phantom was placed on the cover of the kVD, which was facing up during acquisition.

In the low contrast sensitivity measurement, a 1 mm copper plate was placed between kVS and kVD to mimic the attenuation through a patient. For OBI, a copper filtration was placed over the kVS, while for XVI, the copper plate was placed on top of the phantom. In both tests, the X-ray collimation were set to maximum. The X-ray parameters used for each tests are shown in Table 4.3.1.

Figure 4.6: The TOR 18FG Leeds phantom (left) and its kV planar image (right). High contrast resolution and low contrast sensitivity modules are located in the central and peripheral region of the phantom, respectively.[46]

Table 4.3.1: The X-ray parameters used in the planar kV images with the Varian OBI and Elekta XVI units.[47]

Measurement	Varian OBI	Elekta XVI
High Contrast Resolution	50 kVp 50 mA 6 ms 0.3 mAs	70 kVp 50 mA 10 ms 0.5 mAs
Low Contrast Sensitivity	75 kVp 25 mA 4 ms 0.1 mAs	70 kVp 25 mA 10 ms 0.25 mAs

4.3.2 CBCT Image

All CBCT imaging quality tests for the OBI and the XVI units were carried out using a Catphan® 500 phantom (model: CTP 504, The Phantom Laboratory, Salem, NY) (Figure 4.7a). The CTP 504 phantom is cylindrical with 20 cm length and 20 cm diameter and is composed of several modules that measure different aspects of CBCT image quality (Figure 4.7b). During measurements, the phantom was placed at the end of the treatment couch, leveled, and aligned with the isocenter of the treatment beam. The reconstructed images were saved and exported as DICOM files, which were then analyzed using OsiriX software v.5.8.2.[48] Five aspects of image quality were assessed: high contrast resolution, Hounsfield Unit (HU) accuracy, spatial linearity, low contrast sensitivity, and image uniformity.

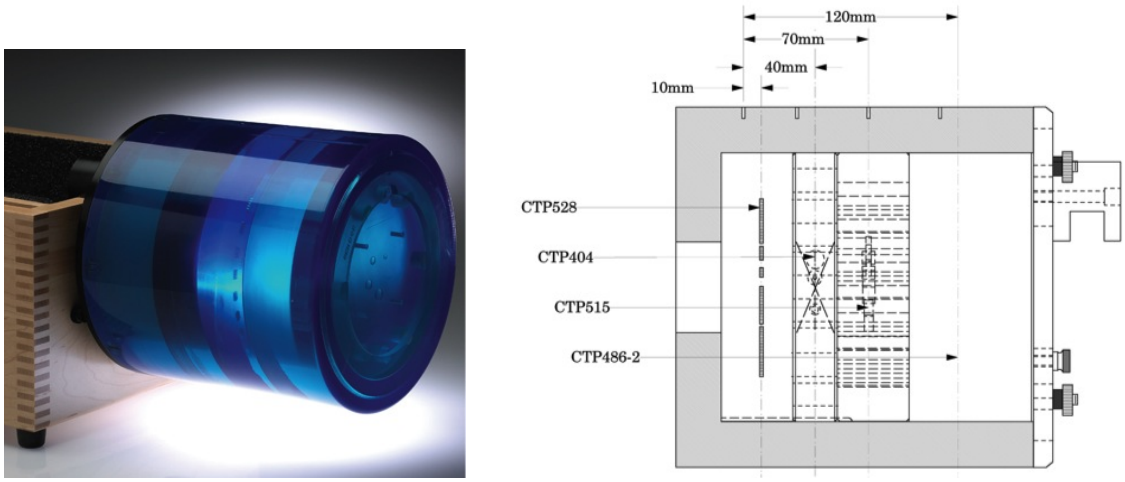

(a) (b)

Figure 4.7: (a) Catphan®500, (b) Illustration of CTP 504 model.[49,50]

Module CTP528 (Figure 4.8a) was used to measure high contrast resolution. It consists of 21 line pair patterns ranging from 1 to 21 line pairs per centimeter (lp/cm).

The high contrast resolution was determined by counting the maximum number of line pairs that could be visualized.

CTP404 module (Figure 4.8b) was used to measure the HU values; it has seven different inserts each with known densities and attenuation coefficients: teflon, delrin, acrylic, polystyrene, low density polyethylene (LDPE), polymethylpentene (PMP), and air. The CT number, or HU value, is defined as

$$\text{CT\#} = \frac{(\mu_{\text{tissue}} - \mu_{\text{water}})}{\mu_{\text{water}}} \times 1000 \tag{4.1}$$

where μ_{tissue} and μ_{water} are the linear attenuation coefficients for a tissue sample and water, respectively. HU values of air, acrylic, and LDPE were recorded and compared to their nominal values as listed in Table 4.3.2. The measured HU values of each material should be within ±40 HU of the nominal values.[47]

Table 4.3.2: Some of the materials present in CTP 404 module and their nominal CT numbers with comparison to water.[47,49]

Material	Formula	Nominal CT #
Air	.78N, .21O, .01Ar	-1000
LDPE	C_2H_4	-100
Water	H_2O	0
Acrylic	$C_5H_8O_2$	120

The same module was used to check spatial linearity. The goal of this test is to make sure that the reconstructed image accurately represents the phantom dimension. There are four rods (three air and one Teflon) located at the corners of a 50 mm square in the middle of the CTP404 module. The measuring tool in OsiriX was used to measure the distance in the x and y directions between the four rods. The average distance was determined and recorded for each scanning protocol. The measured distances should be within ±0.5 mm (±1%) of the reference value (50 mm).

The low contrast sensitivity test was to quantify how well the CBCT system is able to distinguish two objects with minimal difference in contrast. CTP515, the low contrast module (Figure 4.8c), is made up of six different contrast target areas that belong to two main groups: supra-slice and sub-slice contrast targets. The supra-slice targets have a diameter ranging from 2 to 15 mm with contrast levels of 0.3%, 0.5%, and 1%, located in the periphery of the phantom. The sub-slice contrast targets, located in the center of the phantom, have diameters of 3, 5, 7, 9 mm and rod length of 3, 5, 7 mm. The smallest diameter and contrast level visible on an image are indicative of the low contrast sensitivity.

Module CTP486-2 was used to evaluate image uniformity. It is made of uniform material within 2% of the density of water (±20 HU). Five regions of interest (ROI) were selected at different locations (Figure 4.8d) and HU values were measured. In addition, the maximum difference between the HU value of the center ROI and those of peripheral ROIs was also recorded. The measured HU values for all regions as well as the maximum difference as defined above should be within ±40 HU.

It is to be noted that the 2D and 3D high contrast resolution and low contrast sensitivity tests are visual tests. In other words, the visibility of bar patterns and contrast targets might differ from one observer to another. The examination of the images will also be affected by the window level, zoom functions, and the users vision and perception.

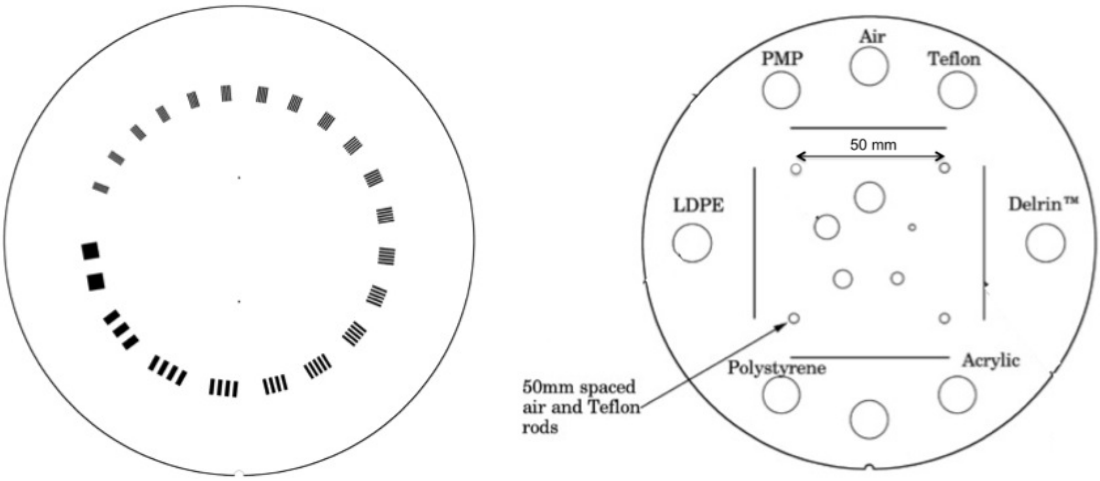

(a) CTP 528

(b) CTP 404

(c) CTP 515

(d) CTP 486-2

Figure 4.8: The modules of the Catphan phantom (model: CTP 504).[49]

4.4 CBCT Dose

It is important to quantify the additional dose associated with imaging. Computed Tomography Dose Index (CTDI) method was used in this study to estimate absorbed dose. In 1981, CTDI was introduced in the USA by the Food and Drug Administration (FDA) to describe dose in a single slice. CTDI is defined as the the integral over the dose profile along a straight line parallel to the axis of rotation, divided by slice thickness and number of slices.[51]

$$\mathrm{CTDI}_{100} = \frac{1}{N \cdot T} \int_{-50\mathrm{mm}}^{+50\mathrm{mm}} D(z)dz \quad [\mathrm{mGy}] \tag{4.2}$$

where N denotes the number of slices measured, T refers to the slice thickness, and $D(z)$ represents the dose distribution along the z-axis. The integration limits are chosen from -50 mm to +50 mm for a single slice CT image since dose at 50 mm or more was negligible. The readouts from an ion chamber gives the value of the CTDI_{100}. Taking into account that dose distribution in a CTDI phantom decreases in direction from surface to center, the weighted CTDI can be approximated by

$$\mathrm{CTDI}_{\mathrm{w}} = \left(\frac{1}{3}\right) \cdot \mathrm{CTDI}_{\mathrm{central}} + \left(\frac{2}{3}\right) \cdot \mathrm{CTDI}_{\mathrm{peripheral}} \quad [\mathrm{mGy}] \tag{4.3}$$

Here $\mathrm{CTDI}_{\mathrm{central}}$ is measured at the central axis of the phantom and $\mathrm{CTDI}_{\mathrm{peripheral}}$ is the average of four different CTDI values measured in the periphery areas of the phantom. It should be noted that the CTDI value does not represent the dose to a specific patient, but used to quantify output of a CT scanner.

In order to estimate the $\mathrm{CTDI}_{\mathrm{w}}$, head and body phantoms were used (Figure 4.9). The cylindrical phantoms are made of polymethyl methacrylate (PMMA) with density

of 1.18 g/cm^3. The head phantom has a diameter of 16 cm and the body phantom has a diameter of 32 cm. Both phantoms have a length of approximately 16 cm. During the measurement, the phantom was placed on the treatment couch and aligned at the isocenter using the room lasers.

CTDI was measured with an electrometer (Model: 9015, Radcal Corporation Radiation, Monrovia, CA) and a 3 cm^3 ion chamber (Model: 10X5-3CT, Radcal). The electrometer was calibrated to give measured doses in units of air kerma (mGy). The active length of the ion chamber was 100 mm. For each measurement of CTDI, the ion chamber was inserted at the center axis of the phantom and then at each of the four peripheral locations. Five insertion locations were labeled as center, 3, 6, 9, and 12 o'clock positions. When the ion chamber was inserted in one location, the others were filled with PMMA rods to eliminate air cavities.

In the XVI units, the head phantom was scanned with head and neck scanning protocols and the body phantom was measured with pelvis and prostate protocols. Detailed scan settings are shown in Table 4.4.1. Using the OBI units, the head phantom was measured with high-quality and standard-dose head protocols while the body phantom was scanned with pelvis and low-dose thorax protocols. Note that in the head protocols full-fan scan technique was used, while in the other protocols, half-fan scan mode was used. Table 4.4.2 contains a complete description of the OBI system settings used for each protocol.

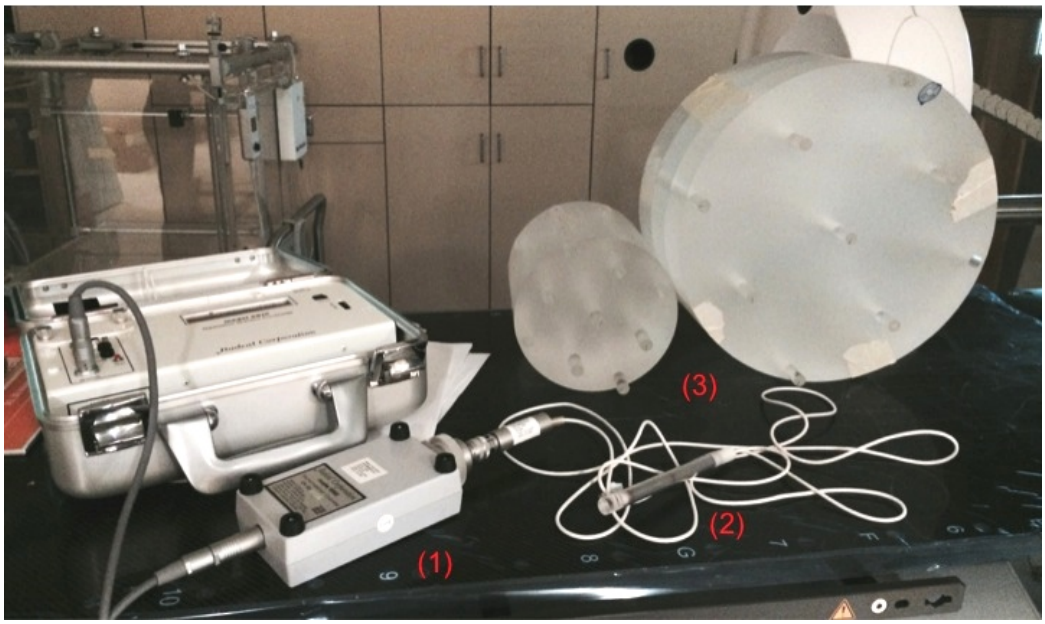

Figure 4.9: The necessary tools used for measuring CBCT dose. (1) Radcal dose monitor (electrometer), (2) Radcal CTDI ion chamber, and (3) head and body phantoms.

Table 4.4.1: Detailed CBCT parameters of the XVI system as well as the $CTDI_w$ values from the XVI reference guide.[44]

	Head and Neck (Fast)	Head and Neck (Standard)	Pelvis	Prostate
kV Collimator	S20	S20	M20	M10
X-Ray Voltage [kVp]	100	100	120	120
Tube Current [mA]	10	10	40	64
Exposure Time [ms]	10	10	40	40
Number of Projections	185	366	660	660
Exposure [mAs]	18.5	36.6	1056	1689.6
Reference $CTDI_w$ [mGy]	0.5	1.1	19.3	28.5
Bow-Tie Filter	F0	F0	F1	F1

Table 4.4.2: Detailed CBCT parameters of the Varian OBI system as well as the $CTDI_w$ values from the OBI reference guide.[40]

	Standard-dose head	High-quality head	Pelvis	Low-dose thorax
X-Ray Voltage [kVp]	100	100	125	110
Tube Current [mA]	20	80	80	20
Exposure Time [ms]	20	25	13	20
Gantry Rotation [deg]	200	200	360	360
Number of Projections	360	360	655	655
Exposure [mAs]	145	720	680	262
Reference $CTDI_w$ [mGy]	3.9	19.4	17.7	4.7
Fan Type	Full fan	Full fan	Half fan	Half fan
Bow-Tie Filter	Full	Full	Half	Half

Chapter 5

Results

Using the methods described in the previous chapter, the image quality and CBCT dose were assessed for both the Varian OBI and Elekta XVI systems for different imaging techniques (refer to Table 4.4.1 and Table 4.4.2).

5.1 Image Quality

5.1.1 Planar kV Image

Figures 5.1 and 5.2 show the planar kV images of the Leeds phantom using Varian OBI and Elekta XVI systems. For the high contrast resolution test (Figure 5.1) , both systems were capable of resolving 1.6 lp/mm (11th bar pattern). For low contrast sensitivity measurements (Figure 5.2), Clinac 4 unit was able to resolve a minimum of 2.01% contrast sensitivity (disk #13), while at Clinac 5 disk #12 (2.33% sensitivity) was barely visible. Elekta XVI system provided slightly better low contrast sensitivity as compared to OBI. Infinity 2 was able to resolve up to disk #14 with contrast

sensitivity of 1.61%, while in Infinity 1 disk #13 was visible. It should be noted that XVI images appeared smaller than OBI due to the limited size of the copper plate placed on top of the phantom as shown in Figure 5.2.

5.1.2 CBCT Image

A. High contrast resolution

The CBCT images of the high contrast resolution module using the Varian OBI and Elekta XVI systems are shown in Figures 5.3 and 5.4. For the OBI, 7 lp/cm was visible for standard-dose head protocol, while 4 lp/cm was visible for pelvis protocol. For the XVI, 4 lp/cm was visible for both protocols. No difference was observed between Clinac 4 and 5 nor between Infinity 1 and 2.

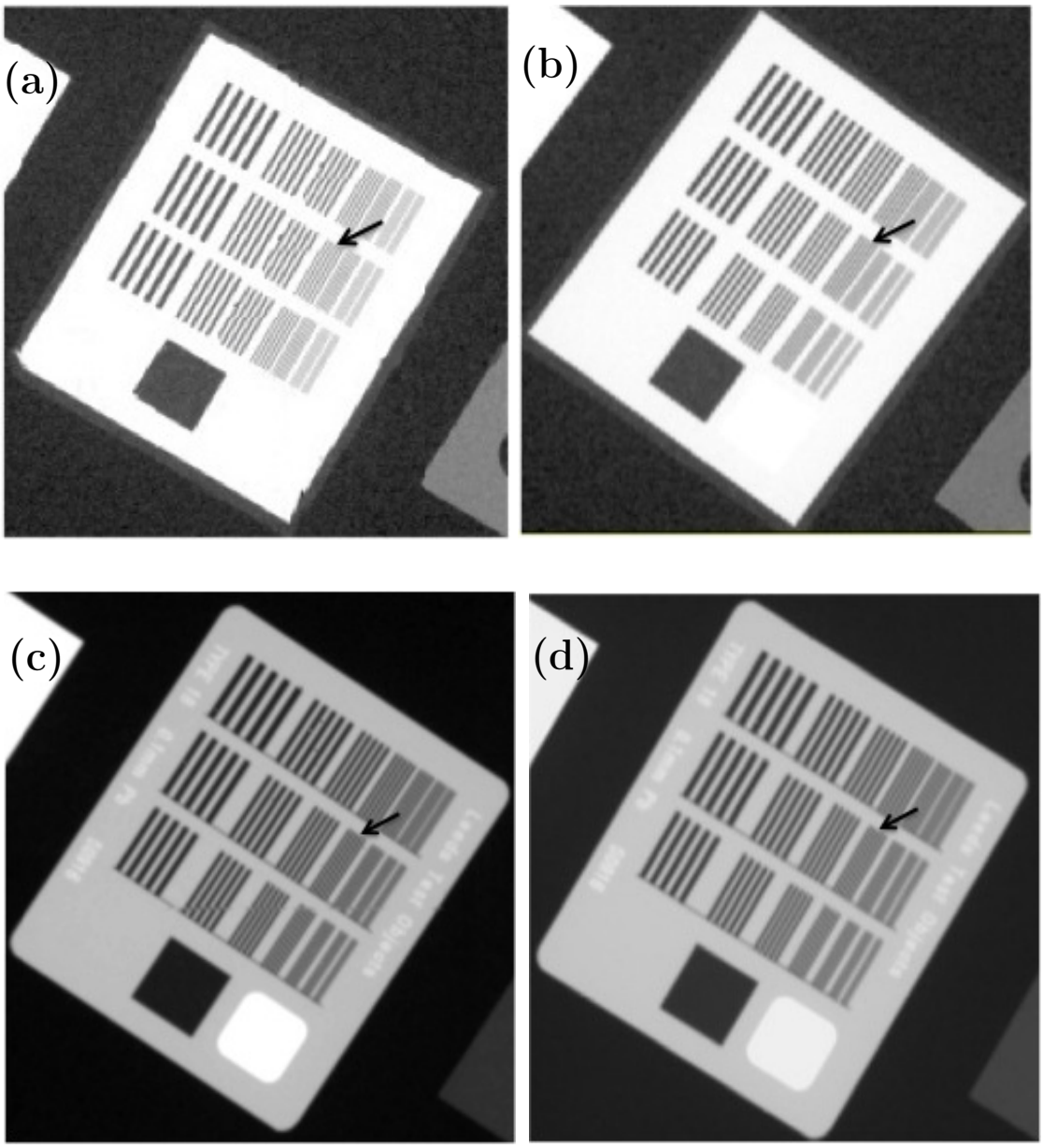

Figure 5.1: Planar images showing the high contrast resolution for (a) Clinac 4, (b) Clinac 5, (c) Infinity 1, and (d) Infinity 2. The arrow shown in each figure represents the 11th bar pattern.

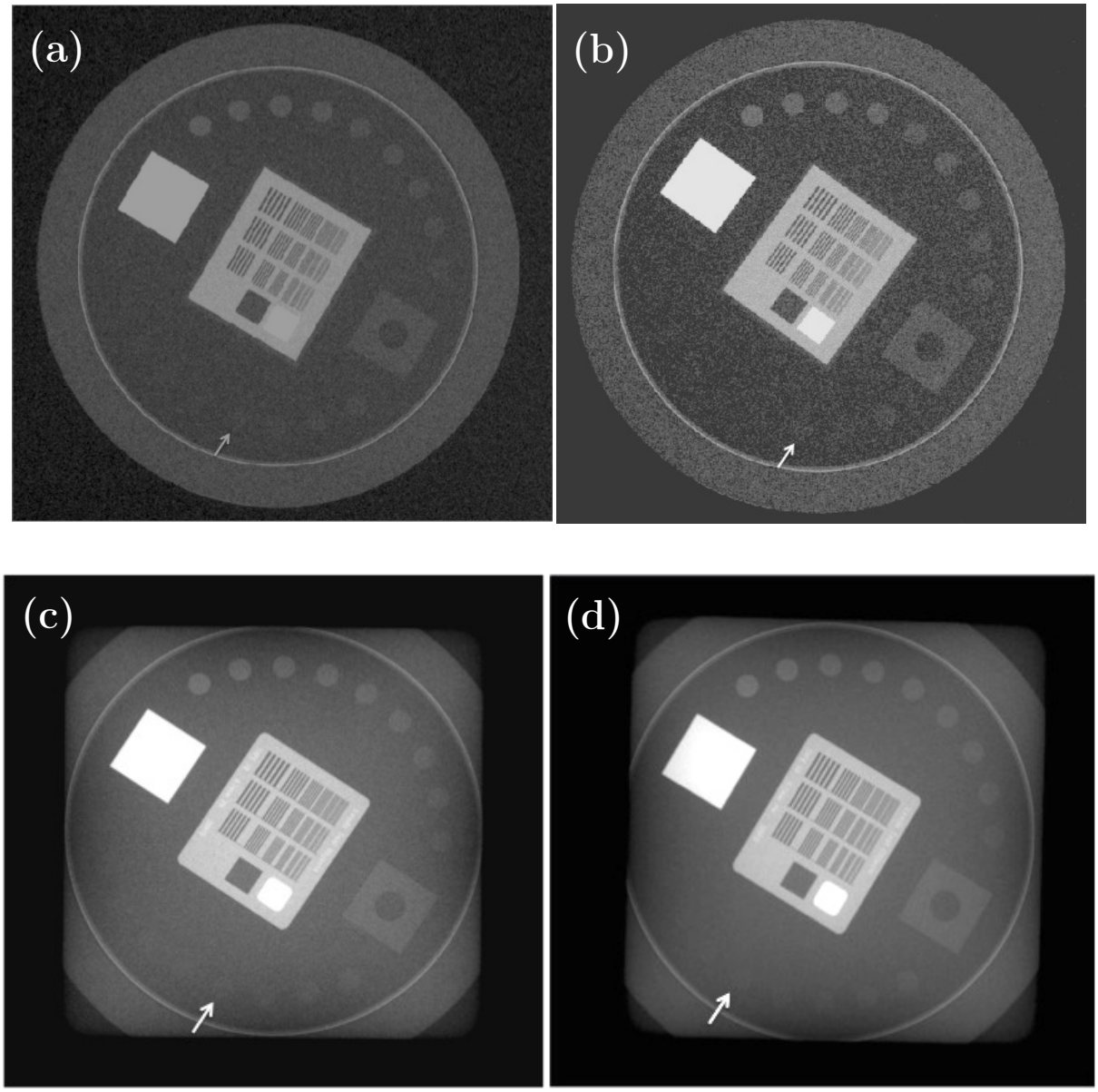

Figure 5.2: Planar images showing the low contrast sensitivity. (a) Clinac 4, (b) Clinac 5, (c) Infinity 1, and (d) Infinity 2. The arrow shown in each figure represents the maximum disk reported.

Pelvis Protocol

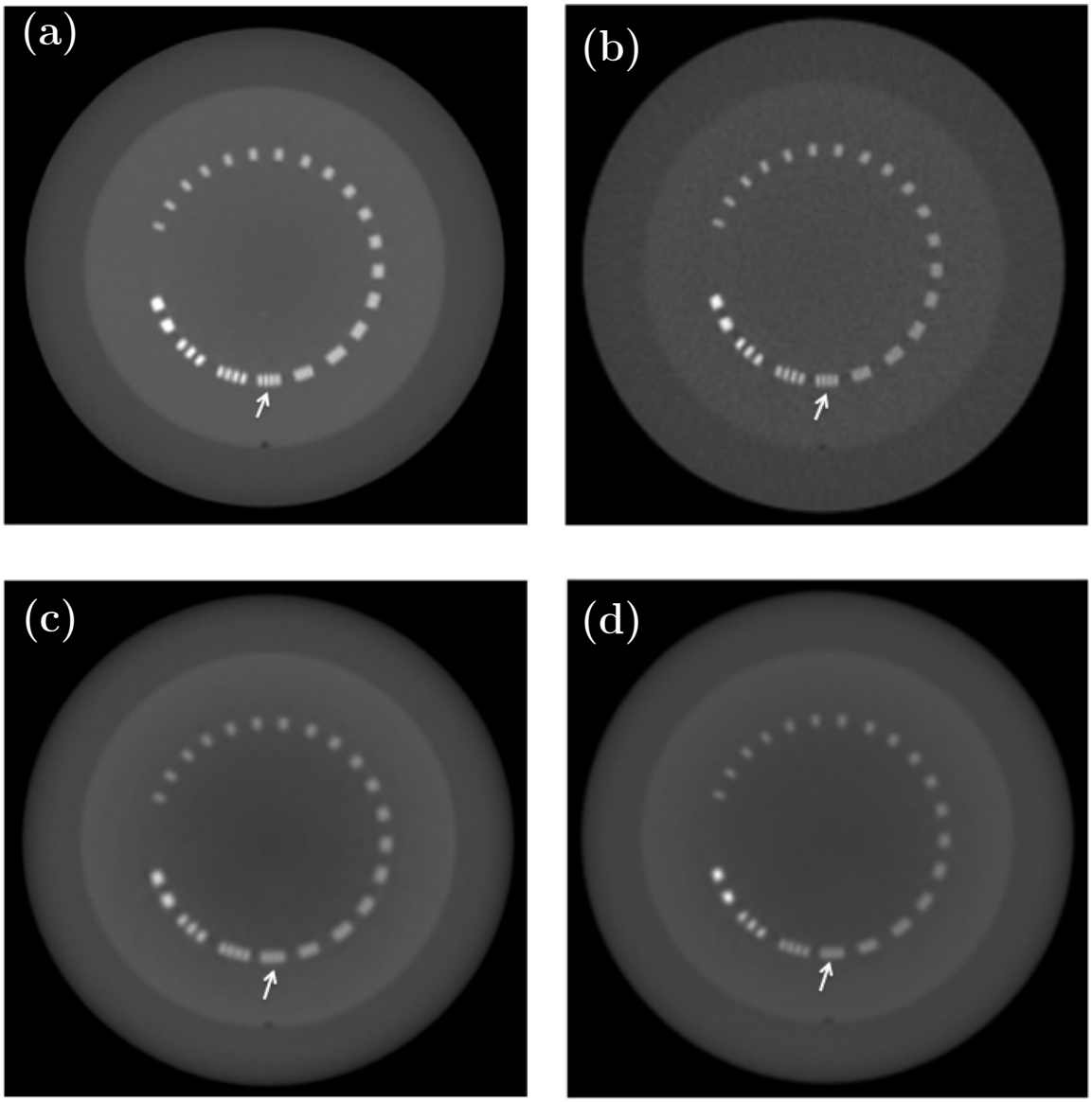

Figure 5.3: Images of high contrast resolution module using pelvis protocol for (a) Clinac 4, (b) Clinac 5, (c) Infinity 1, and (d) Infinity 2. The arrow shown in each figure represents the maximum lp/cm reported for pelvis protocol.

Standard-Dose Head Protocol

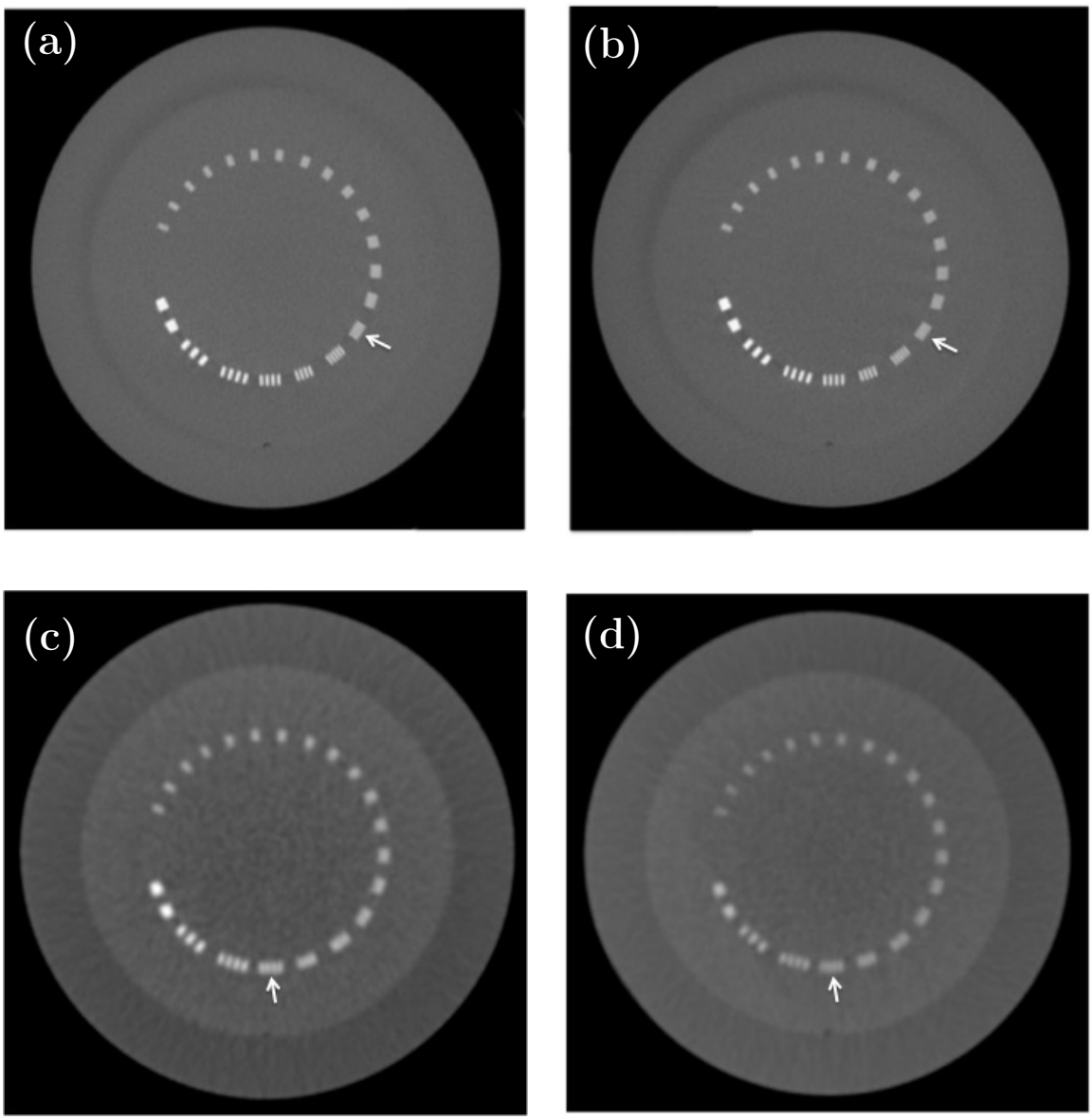

Figure 5.4: Images of high contrast resolution module using standard-dose head protocol for (a) Clinac 4, (b) Clinac 5, (c) Infinity 1, and (d) Infinity 2. The arrow shown in each figure represents the maximum lp/cm reported for head protocol.

B. Hounsfield Unit (HU) accuracy

The accuracy of HU values is presented in Table 5.1.1 for the OBI and XVI units. The table shows the measured HU values for air, acrylic, and LDPE for two scanning protocols, standard-dose head and pelvis, as well as the reference HU for each material.

For the OBI system, the measured HU values for air were within 2 to 6 HU of the reference values. The largest deviation was shown in the head protocol acquired on Clinac 4, where a value of -994 was recorded. The HU values measured in both units were well within tolerance (± 40 HU).

The measured HU values for acrylic and LDPE were also consistent with the reference HU. Clinac 4 data showed a good agreement with the reference values of HU with a deviation of less than 3 HU (including head and pelvis protocols) in both materials. For Clinac 5, the largest deviations of 34 and 38 HU from the reference HU values (120 and -100) were found in the pelvis protocol, where HU of 86 and -138 were recorded for acrylic and LDPE, respectively. Deviation of the HU values in the head protocol was smaller.

The reported HU values for XVI units were not consistent with the reference HU values for all materials since the XVI system was not calibrated for HU values. It is to be noted that HU calibration was not available in the current XVI software version 4.5, which was used in this study. This explains the poor HU accuracy shown in Table 5.1.1.

Table 5.1.1: The measured HU values using Varian OBI and Elekta XVI systems for two different imaging protocols.

Material	Reference HU ± tolerance	**Standard-Dose Head Protocol**				**Pelvis Protocol**			
		OBI units		**XVI units**		**OBI units**		**XVI units**	
		Clinac 4	Clinac 5	Infinity 1	Infinity 2	Clinac 4	Clinac 5	Infinity 1	Infinity 2
Air	-1000 ±40	-994	-998	-545	-525	-1000	-999	-937	-945
Acrylic	120 ±40	123	122	278	293	120	86	-279	-276
LDPE	-100 ±40	-102	-121	126	133	-101	-138	-400	-406

C. Spatial linearity

The distances between air and Teflon rods were measured using CTP404 module in the Catphan phantom, in which the nominal distance is equal to 50.0 mm. For OBI units, the measured distances between the rods ranged from 50.0 mm to 50.2 mm with half-fan mode (pelvis protocol), and from 49.8 mm to 50.0 mm with full-fan mode (head protocol). For XVI units, the measured distance ranged from 49.5 mm to 50.3 mm for the head protocol, while for pelvis protocol, the measured distance ranged from 49.1 mm to 49.7 mm.

D. Low contrast sensitivity

The low contrast sensitivity was measured in the CTP515 module of the Catphan phantom for both types of imaging system. The number of visible disks in the pelvis images was evaluated and presented in Figure 5.5 for both the Varian OBI and Elekta XVI systems. It should be noted that this test does not apply to the head protocol since it uses much less dose than the pelvis protocol. Please refer to Table 4.4.1 and Table 4.4.2 for more details. For both types of system, five out of the nine disks (15, 9, 8, 7, 6 mm diameters) at 1 % target contrast level were visible. For OBI images, disks at 0.5 % contrast level were barely visible, while disks at 0.3 % contrast level were totally invisible. None of the 0.5% and 0.3% disks were visible on the XVI images.

Pelvis Protocol

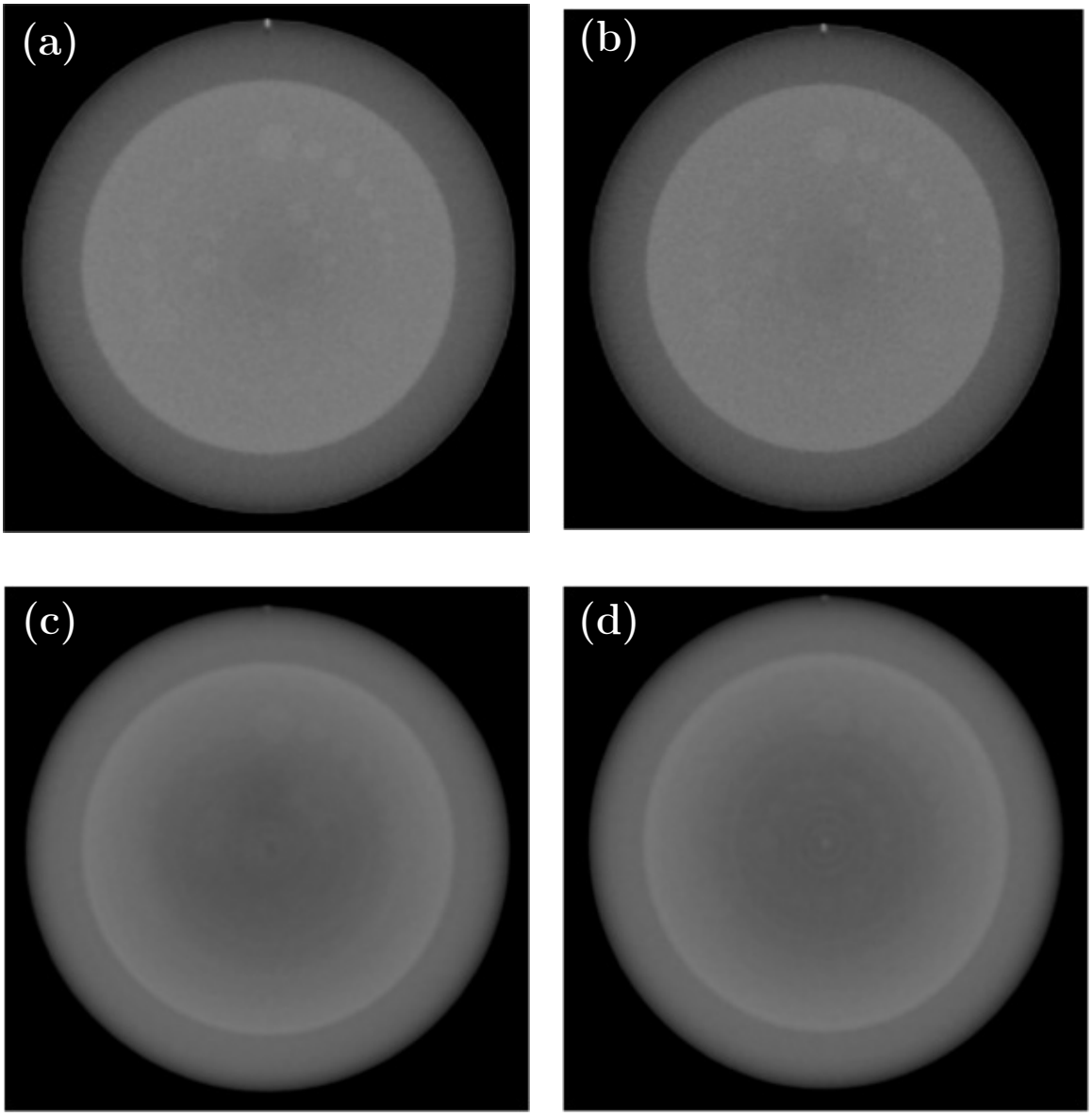

Figure 5.5: Images of the low contrast sensitivity module using pelvis protocol for (a) Clinac 4, (b) Clinac 5, (c) Infinity 1 and (d) Infinity 2.

E. Image uniformity

HU values in five regions of interest (ROI) were measured in the CTP486-2 module of the phantom to determine image uniformity. Table 5.1.2 summarizes the HU values in five ROIs as well as the maximum HU differences between the central and peripheral ROIs with head and pelvis protocols using OBI and XVI systems. For Varian OBI, the maximum HU differences were well below the tolerance (±40 HU) for both units using both protocols.

Using standard-dose head protocol, the maximum HU differences were 33 and 12 for Infinity 1 and 2, respectively. However, using pelvis protocol, the maximum HU differences were -59 and -52, exceeding the tolerance of ±40 HU.

Table 5.1.2: HU values in ROIs in the uniformity module in the Catphan phantom using Varian OBI and Elekta XVI systems, respectively. The maximum HU differences for both types of system are also shown.

ROI locations	**Standard-Dose Head Protocol**				**Pelvis Protocol**			
	OBI units		**XVI units**		**OBI units**		**XVI units**	
	Clinac 4	Clinac 5	Infinity 1	Infinity 2	Clinac 4	Clinac 5	Infinity 1	Infinity 2
Center	22.21	11.69	206	226	3.20	-36.34	-387	-388
Left	13.09	0.39	214	228	2.03	-30.47	-329	-338
Top	10.11	1.51	239	251	1.71	-31.07	-328	-337
Right	7.56	4.17	212	223	1.86	-23.92	-337	-337
Bottom	10.98	0.60	210	214	1.12	-24.12	-331	-336
Max difference (HU)	**14.65**	**11.30**	**33**	**25**	**2.08**	**-12.42**	**-59**	**-52**

5.2 CBCT Dose

5.2.1 Varian OBI measurements

Table 5.2.1 represents the measured dose at different positions of CTDI phantoms using the two different units of OBI system, Clinac 4 and Clinac 5, respectively. Dose measurements were conducted for four clinical protocols. The results of this study were compared to results published by Varian for the OBI[40] and by Hyer *et al.*[52] The scan parameters of each of these protocols can be found in Table 4.4.2.

Table 5.2.1: Measured dose on the CTDI head and body phantoms for various CBCT protocols using Varian OBI system.

Protocol	High-quality head	Standard-dose head	Pelvis	Low-dose thorax
Dose [mGy]		**Clinac 4**		
D_{center}	28.38	5.92	16.44	4.46
12 o'clock	9.58	1.99	29.23	8.79
3 o'clock	23.59	4.97	29.83	8.66
6 o'clock	41.47	8.58	28.70	8.26
9 o'clock	33.74	7.04	29.50	8.57
$D_{peripheral}$	27.10	5.65	29.32	8.58
$CTDI_w$[mGy]	**27.52**	**5.74**	**25.02**	**7.20**
Dose [mGy]		**Clinac 5**		
D_{center}	26.34	5.34	14.18	3.91
12 o'clock	9.17	1.83	25.05	7.19
3 o'clock	22.39	4.54	24.25	7.00
6 o'clock	37.76	7.71	23.34	6.76
9 o'clock	31.01	6.31	24.86	7.16
$D_{peripheral}$	25.08	5.10	24.38	7.03
$CTDI_w$[mGy]	**25.50**	**5.18**	**20.98**	**5.99**
Reference $CTDI_w$[mGy][a]	**19.4**	**3.9**	**17.7**	**4.7**
Hyer *et al.*[52]	**-**	**5.17**	**21.57**	**6.14**

[a] Data from the Varian OBI reference guide shown for comparison.[40]

5.2.2 Elekta XVI measurements

Tables 5.2.2 and 5.2.4 summarize the dose measurements, at the center and peripheral locations in the head and body phantoms, conducted for four different protocols using the XVI units (Infinity 1 and 2). The $CTDI_w$ results performed by Elekta for XVI and Song *et al.* are also shown in both tables.

Table 5.2.2: Measured dose on the CTDI head and body phantoms for various CBCT protocols using Elekta XVI system.

Protocol	Fast head and neck (S20)	Standard head and neck (S20)	Pelvis (M20)	Prostate (M10)
Dose [mGy]		**Infinity 1**		
D_{center}	0.43	0.77	13.20	18.99
12 o'clock	0.25	0.50	22.95	33.24
3 o'clock	0.57	1.12	22.21	33.33
6 o'clock	0.78	1.50	22.41	31.64
9 o'clock	0.51	0.94	24.14	37.16
$D_{peripheral}$	0.53	1.01	22.93	33.84
$CTDI_w$[mGy]	**0.50**	**0.93**	**19.68**	**28.89**
Dose [mGy]		**Infinity 2**		
D_{center}	0.40	0.80	13.39	18.55
12 o'clock	0.24	0.50	22.06	36.24
3 o'clock	0.50	1.05	22.83	32.36
6 o'clock	0.71	1.46	22.42	32.37
9 o'clock	0.46	0.93	25.80	39.73
$D_{peripheral}$	0.48	0.99	23.27	35.17
$CTDI_w$[mGy]	**0.45**	**0.92**	**19.98**	**29.63**
Reference $CTDI_w$[mGy][a]	**0.50**	**1.10**	**19.30**	**28.50**
Song *et al.*[32]	**-**	**1**	**24**	**35**

[a] Data from the Elekta XVI reference guide shown for comparison.[44]

Chapter 6

Discussion

The purpose of this study was to give a quantitative comparison of image quality and CBCT dose analysis between Varian OBI and Elekta XVI systems while using the standard clinical imaging protocols on both systems. Image quality phantoms, TOR 18FG Leeds and Catphan, were useful tools in quantifying the results of the 2D and 3D image quality tests from the OBI and XVI systems. A comprehensive set of CBCT dose measurements were also performed for OBI and XVI systems using CTDI head and body phantoms.

6.1 Planar kV image

The measured 2D high contrast resolution for the OBI and XVI units was consistent with one another; 1.6 lp/mm was recorded for both systems (4 units). For OBI images, the measured values were in good agreement with the values reported by Yoo *et al.* even though their exposure was much higher (≈2.56 mAs) than the one used in this study (0.3 mAs).[41] The high contrast resolution of XVI units was lower

than the values reported by Muralidhar *et al.*, in which 2.2 lp/mm (13th bar pattern) was recorded.[53] For the low contrast sensitivity test, the XVI showed better contrast detectability than the OBI system due to the higher mAs value of the XVI units. Also, image noise was found on the OBI images due to the low dose as shown in Table 4.3.1. The OBI units were capable of resolving twelve to thirteen disks (2.33% to 2.01% contrast sensitivity), which was similar to the values reported by Yoo *et al.* For XVI units, the reported values of the low contrast test were lower than Muralidhar *et al.*'s values (disk #16). In general, 2D image quality results for both machines met the required specifications recommended by manufacturers.[47,54]

6.2 CBCT image

Before discussing CBCT image quality results, it is important to review some factors affecting the image quality on OBI and XVI systems. First of all, the OBI uses a full bow-tie filter with the full-fan scan, while XVI has no bow-tie filter for the same scan. A shaped filter decreases the dynamic range demands on the detector during a CBCT image acquisition. Also, it reduces the scatter signal at the phantom's edge which leads to improved overall quality of the CBCT images.[45] For these reasons, one may expect better image quality on the OBI system than XVI. Secondly, image reconstruction settings might affect the quality of CBCT images. XVI has three different presets for reconstruction: high, medium, and low resolution. The major difference between these presets is the reconstruction voxel size. For small and medium FOV settings (S20&M10 cassettes), the voxel sizes for the high, medium, and low reconstruction

presets are $(0.5)^3$, $(1)^3$, and $(2)^3$ in units of mm^3, respectively.[55] In this study, the medium resolution setting was used for all CBCT protocols since this is the one that is usually used clinically. The high resolution setting is not common for clinical use because it takes approximately 2 minutes longer to reconstruct the image. However, it should be noted that the high resolution reconstruction preset will improve some quality parameters of CBCT images due to the smaller voxel size. Furthermore, the CBCT dose affects the overall image quality. Insufficient dose results in increased noise and reduction of image quality, while an increase in dose over a certain level results in unnecessarily high dose to the patient without clinical benefit from improved image quality.

The CBCT high contrast resolution is dependent on many factors, which is why direct comparison between the Varian OBI and Elekta XVI is difficult. Looking at the pelvis protocol images, both systems were capable of resolving 4 lp/cm. The OBI images for head protocol had higher resolution than XVI images because the OBI system used higher dose and smaller pixel/voxel size. An increase in image noise was found on the XVI images due to the low dose. Resolution is clearly limited by dose, pixel size, and therefore SNR. In CT, there is a well-established relationship between dose (D), SNR, pixel size (Δ), and slice thickness (T), namely[4]

$$\mathrm{D} \propto \frac{\mathrm{SNR}^2}{\Delta^3 \mathrm{T}} \tag{6.1}$$

Resolution will be affected by the pixel size, which is dependent on FOV and reconstruction pixel matrix. For example, in the full-fan mode of the OBI, a 384×384 matrix with FOV of 25 cm resulted in pixel dimensions of approximately 0.7 mm,

implying a maximum resolution that can be conveyed in the image (the Nyquist frequency) of $(2\times0.7\text{ mm})^{-1}$, or 7 lp/cm, while for the XVI full-fan mode, a 1 mm pixel size imposed a maximum resolution of 5 lp/cm. Further improvement in the high contrast resolution was also shown on the full-fan mode on OBI because it used a sharp reconstruction filter, which emphasizes on bony structures, in its imaging process which may lead to better resolution.

HU values can vary significantly between different imaging protocols and scanners, it was important to check if the reference and the measured HU are comparable to each other for both OBI units. In this study, it is shown that the HU values varied randomly between the two units. Looking at Table 5.1.1, there are relatively large differences in HU values between the protocols used on each unit. For instance, the HU difference between the measured and nominal values in LDPE for the CBCT pelvis protocol using Clinac 5 is 37.96, while for Clinac 4 the difference is only 1. Larger discrepancy, though still within tolerance of ±40 HU, could likely be improved with a HU re-calibration. As mentioned earlier, the reported HU values for XVI units were not accurate since pixel values were not calibrated to the realistic HU values during the installation and acceptance procedure. It is to be noted that the XVI version used in this study (v4.5) does not support HU calibration; however, the newest version of XVI (v5.0) does support this type of calibration.

For dose calculation, HU values are converted to electron densities by using calibration curve. In this study, for HU accuracy and image uniformity tests, a tolerance in HU values of ±40 was used, which will translate to 4% of density of water. Within

this range, the inaccuracy of dose calculation is expected to be small.

The geometric accuracy of CBCT systems is influenced by the divergence of the X-ray beam. The CBCT images are considered geometrically consistent if the actual divergence of the beam agrees with that assumed in the reconstruction. Spatial linearity test was conducted to check the accuracy of the image magnification. It was assessed for both OBI and XVI systems for two different imaging protocols. For OBI system, comparison of the expected and measured distances of the four rods showed excellent agreement, in which all distances were well within tolerance ($\pm 1\%$). For XVI system, the measured distances ranged from 49.5 to 50.3 for head protocol, while for pelvis protocol some of the measured distances were slightly below the tolerance (± 0.5 mm), where 49.1 mm was recorded.

For the low contrast sensitivity test, the low contrast inserts were not visible on either OBI or XVI systems using standard-dose head protocol due to the low dose. The reason for using low radiation dose for head protocols is that the bony structures are sufficient for image guidance in radiotherapy, thus there is no need to use higher dose.[56] Using pelvis protocol, both systems were capable of resolving up to 6 mm diameter 1% supra-slice disk. The 0.5 and 0.3 % supra-slice disks were more visible on the OBI images than the XVI even though the mAs value for XVI was higher. The mAs affects the number of X-ray photons used to produce the image, therefore affecting the SNR and the low contrast sensitivity (Equation 6.1). The reduction of the low contrast sensitivity of XVI images might be related to the type of reconstruction quality setting used in this study. In general, the CBCT system has limited ability

to detect low-contrast objects and that might be related to significant levels of image noise.

The image noise is an important factor affecting image quality since it both reduces the spatial resolution and low contrast sensitivity. The increase in noise is mainly due to the variation in the number of X-ray photons detected (quantum noise) and/or the type of the reconstruction algorithm.[5] Reducing the quantum noise can be achieved by increasing the number of photons reaching the detector. Using higher mAs will increase the number of photons, which leads to a reduction in the amount of noise. The reconstruction algorithm, which is used to reconstruct images from projections data, uses filters that might also increase the noise in the images. For example, bone filters increase the noise (and thereby reduce low contrast sensitivity), and soft tissue filters improve the low contrast sensitivity by reducing the amount of noise in the images.

The uniformity module in Catphan phantom is designed to measure the CBCT system's ability to produce uniform images across the field of view of an object with uniform density. All OBI images showed good in-slice uniformity with maximum variation between central and peripheral ROIs < 15 HU. For full and half-fan mode, the HU values of the different ROIs were within the expected value for the material (± 40 HU). The center ROI showed a larger HU value and a decrease in the values was seen in the peripheral regions of the images. The full-fan images of the XVI units showed better uniformity than the half-fan mode; variations between ROIs were 33 and 25 HU for Infinity 1 and Infinity 2, respectively. The lower HU value toward

the center in XVI head images might be related to beam hardening correction which can cause cupping artifacts in the images. A large non-uniformity was observed in pelvis images for both units (-52 and -59 HU). This larger discrepancy could likely be related to the HU calibration as discussed earlier.

6.3 CBCT dose

In this study, a comprehensive set of dose measurements was conducted for the OBI and XVI systems. The CTDI was then calculated for both full and half-fan CBCT protocols. The comparison between the two systems showed that the doses from the Varian OBI standard clinical protocols tend to be higher than Elekta XVI protocols for scanning of similar anatomy sites. However, in both systems, the head protocols delivered lower doses compared to body protocols. This is because both systems used a half-rotation scan for head and neck protocols (200°). The image acquisition on both systems started at the posterior region of the head, therefore, superficial organs located on the anterior part (12 o'clock) were not directly exposed to the radiation. For instance, in high-quality head and standard-dose head protocols of OBI units, the anterior part of the head received only approximately one-quarter of the highest dose measured in the head phantom, which was observed on the posterior region of the head, while for XVI, the anterior part received approximately one-third of the posterior dose.

According to OBI results, the highest CTDI value was reported in a high-quality head protocol. This occurs for two reasons. Firstly, the high-quality head protocol

had higher mAs value than standard-dose head and body protocols. The CTDI values for full-fan scan mode were proportional to mAs; the high-quality head protocol required a dose almost five times higher than standard-dose head and low-dose thorax. Secondly, the effect of the phantom's size might be reasonable since a smaller patient size will lead to a greater image acquisition dose.

Overall, the measured doses of OBI units of each protocol were fairly consistent with one another and with the data reported by Hyer *et al.*.[52] Table 5.2.1 shows doses for default scanning protocols in Clinac 4; the measured $CTDI_w$ values were higher than Hyer *et al.*'s data by approximately 4% to 17%. For Clinac 5 (Table 5.2.1), the measured doses were slightly lower than Hyer *et al.*'s data by 1% to 3%. It is to be noted that Hyer *et al.*'s measurements were repeated three times to decrease statistical errors which might lead to these differences.

For both units, the $CTDI_w$ measurements were 20%-50% higher than the results in the Varian reference guide.[40] This is because Varian's measurements were done quite differently. According to the Varian reference guide, the X-ray blades opening was narrowed to 20 mm (12 mm field length and 4 mm blade margin). To account for blade settings uncertainties, the length of the collimated volume was measured from the plot of the full width at half-maximum (FWHM) of the blade opening. The estimated value of the length was then used to correct the reading from the ion chamber given in Gy·cm.

For XVI units, the $CTDI_w$ results agreed well with one another and with the data reported by Elekta reference guide with a largest difference of ≈16% shown in the

standard head protocol used on Infinity 2. Comparing Song *et al.*'s data to the dose results in this study, it was shown that our results were consistent with Song *et al.*'s results. For the standard head protocol, the values reported in this study were lower than Song *et al.*'s value by $\approx 8\%$, while for pelvis and prostate regions, their data were higher by 18% and 15% for Infinity 1 and Infinity 2, respectively. Note that the phantom sizes in Song *et al.*'s study were slightly different than the phantoms used in this study. In Song *et al.*'s study, a 18 cm diameter head phantom and a 30 cm diameter body phantom were used, while in this study, 16 and 32 cm phantoms were used for head and body protocols, respectively. Even though the head phantom in this study was smaller than the one used in Song *et al.*'s study, measurements with their phantom showed higher doses. For the body phantom, Song *et al.*'s values were higher because their phantom was smaller by 2 cm in diameter.

The major limitation of CTDI methodology is that the 100 mm ion chamber used in CTDI measurements will not collect all the primary radiation as well as the scatter signal generated from a single-scan cone beam.[51] This is because the broad geometry of the X-ray beam used for CBCT image acquisition, which exceeds the 100 mm length of the ionization chamber. The use of a small ion chamber (e.g. 0.6 cm^3 Farmer chamber) has been suggested by some authors for CBCT dose measurements.[32,57–59] The Farmer chamber gives a more accurate measurement of the maximum dose at the center of the phantom.[32] More details on how the measurement is done are provided in the literature.[57–60]

Chapter 7

Conclusions

The goal of this research was to investigate the overall quality of CBCT systems in terms of image quality and doses. The implementation of kV-CBCT in IGRT has the advantage of being able to accurately visualize anatomical structures especially soft tissues. A comprehensive set of image quality and dose measurements were performed using different types of phantoms for the two commercially available kV-CBCT systems (Varian OBI and Elekta XVI). The systems were evaluated by performing image quality and dose measurements for four clinical protocols: head and neck, pelvis, prostate, and thorax.

In evaluating the quality of both the OBI and XVI planar images, it was shown that the OBI was capable of providing comparable imaging performance to that of XVI system. In this study, CBCT image quality measurements of the OBI revealed better high contrast resolution and HU accuracy when using head and pelvis protocols.

CBCT dose measurements demonstrated that the XVI used lower doses for both head and body scans than OBI did, which explains the observed differences in image quality that are mentioned earlier. In addition, the head protocols in both systems delivered lower doses compared to body protocols to minimize the exposure of superficial organs to the radiation.

According to the results presented in this study, both systems are suitable for performing image-guided radiotherapy on a daily basis. This technology is considered a useful tool to aid patient positioning for radiation therapy. Radiation doses vary considerably with patient sizes in relation to scanning protocols.[35] Therefore, it is recommended to consider patient-specific clinical imaging protocols, particularly with regards to pediatric patients for whom a higher dose can be predicted. As future Varian OBI and Elekta XVI systems continue to improve their image quality, both have the potential to become even more valuable tools in image-guided radiation therapy.

Bibliography

[1] E. B. Podgorsak, *Radiation Physics for Medical Physicists.* Springer, 2006.

[2] F. M. Khan, *The Physics of Radiation Therapy.* Lippincott Williams & Wilkins, 4th ed., 2010.

[3] H. Johns and J. Cunningham, *The Physics of Radiology.* Charles C. Thomas, Publisher Ltd, 4th ed., 1983.

[4] J. Bushberg, A. Seibert, E. Leidholdt, and J. Boone, *The Essential Physics of Medical Imaging.* Lippincott Williams & Wilkins, 2nd ed., 2002.

[5] P. Allisy-Roberts and J. Williams, *Farr'sPhysics for Medical Imaging.* Saunders-Elsevier, 2nd ed., 2008.

[6] J. Beutel, H. Kundel, and R. V. Metter, *Handbook of Medical Imaging: Volume 1. Physics and Psychophysics.* SPIE, 2000.

[7] B. Alberts, A. Johnson, J. Lewis, M. Raff, K. Roberts, and P. Walter, *Molecualr Biology of The Cell.* Garland Science, 5th ed., 2008.

[8] "Types of Treatment." http://www.cancer.gov/cancertopics/treatment/types-of-treatment.

[9] "What is Radiation Therapy." http://www.cancer.net/navigating-cancer-care/how-cancer-treated/radiation-therapy/what-radiation-therapy, 2013.

[10] R. Timmerman and L. Xing, *Image-Guided and Adaptive Radiation Therapy*. Lippincott Williams & Wilkins, 2010.

[11] E. B. Podgorsak, *Radiation Oncology Physics: A Handbook for Teachers and Students*. IAEA, 2005.

[12] "ICRU Report 50: Prescribing, Recording and Reporting Photon Beam Therapy.," *Bethesda MD, International Commission on Radiation Units and Measurements (ICRU)*, 1993.

[13] "ICRU Report 62: Prescribing, Recording and Reporting Photon Beam Therapy (Supplement to ICRU Report 50).," *Bethesda MD, International Commission on Radiation Units and Measurements (ICRU)*, 1999.

[14] T. R. Mackie, J. Kapatoes, K. Ruchala, W. Lu, C. Wu, G. Olivera, L. Forrest, W. Tome, J. Welsh, R. Jeraj, P. Harari, P. Reckwerdt, B. Paliwal, M. Ritter, H. Keller, J. Fowler, and M. Mehta, "Image guidance for precise conformal radiotherapy," *Int. J. Radiation Oncology Biol. Phys*, vol. 56, no. 1, pp. 89–105, 2003.

[15] D. Verellen, M. D. Ridder, N. Linthout, K. Tournel, G. Soete, and G. Storme, "Innovations in image-guided radiotherapy," *Nature Publishing Group*, vol. 7, pp. 949–960, 2007.

[16] L. Xing, B. Thorndyke, E. Schreibmann, Y. Yang, T. Li, G. Kim, G. Luxton, and A. Koong, "Overview of image-guided radiation therapy," *Medical Dosimetry*, vol. 31, no. 2, pp. 91–112, 2006.

[17] J. Leong, "Use of digital fluoroscopy as an on-line verification device in radiation therapy," *Radiotherapy and Oncology*, vol. 31, no. 9, pp. 985–992, 1986.

[18] M. Zijtveld, M. Dirkx, H. de Boer, and B. Heijmen, "Dosimetric pre-treatment verification of IMRT using an EPID; clinical experience," *Radiotherapy and Oncology*, vol. 81, pp. 168–175, 2006.

[19] D. Verellen, M. D. Ridder, K. Tournel, M. Duchateau, T. Reynders, T. Gevaert, N. Linthout, and G. Storme, "An overview of volumetric imaging technologies and their quality assurance for IGRT," *Acta. Oncologica*, vol. 47, pp. 1271–1278, 2008.

[20] J. Lehmann, J. Perks, S. Semon, R. Harse, and A. Purdy, "Commissioning experience with cone-beam computed tomography for image-guided radiation therapy," *J. Appl. Clin. Med. Phys*, vol. 8, no. 3, pp. 21–36, 2007.

[21] C. McBain, A. Henry, J. Sykes, A. Amer, T. Marchant, C. Moore, J. Davies, J. Stratford, C. McCarthy, B. Porritt, P. Williams, V. Khoo, and P. Price, "X-ray volumetric imaging in image-guided radiotherapy: The new standard in

on-treatment imaging," *Int. J. Radiation. Oncology. Biol. Phys*, vol. 64, no. 2, pp. 625–634, 2006.

[22] J. Bissonnette, P. Balter, L. Dong, K. Langen, D. M. Lovelock, M. Miften, D. Moseley, J. Pouliot, J. Sonke, and S. Yoo, "Quality assurance for image-guided radiation therapy utilizing CT-based technologies: A report of the AAPM TG-179," *Am. Assoc. Phys. Med*, vol. 39, no. 4, pp. 1946–1963, 2012.

[23] R. Den, A. Doemer, G. Kubicek, G. Bednarz, J. Galvin, W. Keane, Y. Xiao, and M. Machtay, "Daily image guidance with cone-beam computed tomography for head-and-neck cancer intensity-modulated radiotherapy: A prospective study," *Int. J. Radiation. Oncology. Biol. Phys*, vol. 76, no. 5, pp. 1353–1359, 2009.

[24] S. Meeks, J. Harmon, K. Langen, T. Willoughby, T. Wagner, and P. Kupelian, "Performance characterization of megavoltage computed tomography imaging on a helical tomotherapy unit," *Med. Phys*, vol. 32, no. 8, pp. 2673–2681, 2005.

[25] W. W. K. Fung and V. W. Wu, "image-guided radiation therapy using computed tomography in radiotherapy," *Journal of Radiotherapy in Practice*, vol. 10, pp. 121–136, 2011.

[26] E. Klein, J. Hanley, J. Bayouth, F. Yin, W. Simon, S. Dresser, C. Serago, F. Aguirre, L. Ma, B. Arjomandy, C. Liu, C. Sandin, and T. Holmes, "Task Group 142 report: Quality assurance of medical accelerators," *Am. Assoc. Phys. Med*, vol. 36, no. 9, pp. 4197–4212, 2009.

[27] J. Bissonnette, "Quality assurance for image-guidance technologies," *Seminars in Radiation Oncology*, vol. 17, pp. 278–286, 2007.

[28] P. Downes, R. Jarvis, E. Radu, I. Kawrakow, and E. Spezi, "Monte carlo simulation and patient dosimetry for a kilovoltage cone-beam CT unit," *Med. Phys*, vol. 36, no. 9, pp. 4156–4167, 2009.

[29] J. Sykes, R. Lindsay, G. Iball, and D. Thwaites, "Dosimetry of CBCT: methods, doses and clinical consequences," *J. Phys*, vol. 444, pp. 1–13, 2013.

[30] D. E. Hyer, C. F. Serago, S. Kim, J. G. Li, and D. E. Hintenlang, "An organ and effective dose study of XVI and OBI cone-beam ct systems," *J. App. Med. Phys*, vol. 11, no. 2, pp. 181–197, 2010.

[31] M. Kan, L. Leung, W. Wong, and N. Lam, "Radiation dose from cone beam computed tomography for image-guided radiation therapy," *Int. J. Radiation. Oncology. Biol. Phys*, vol. 70, no. 1, pp. 272–279, 2008.

[32] W. Y. Song, S. Kamath, S. Ozawa, S. A. Ani, A. Chvetsov, N. Bhandare, J. Palta, C. Liu, and J. Li, "A dose comparison study between XVI and OBI CBCT systems," *Med. Phys*, vol. 35, no. 2, pp. 480–486, 2008.

[33] A. Amer, T. Marchant, J. Sykes, J. Czajka, and C. Moore, "Imaging doses from the Elekta Synergy x-ray cone beam CT system," *The British Journal of Radiology*, vol. 80, pp. 476–482, 2007.

[34] M. Islam, T. Purdie, B. Norrlinger, H. Alasti, D. Moseley, M. Sharpe, J. Siewerdsen, and D. Jaffray, "Patient dose from kilovoltage cone beam computed tomog-

raphy imaging in radiation therapy," *Med. Phys*, vol. 33, no. 6, pp. 1573–1582, 2006.

[35] E. Nickoloff, A. Dutta, and Z. Lu, "Influence of phantom diameter, kvp and scan mode upon computed tomography dose index," *Med. Phys*, vol. 30, pp. 395–402, 2003.

[36] D. Létourneau, J. Wong, M. Oldham, M. Gulam, L. Watt, D. Jaffray, J. Siewerdsen, and A. Martinez, "Cone-beam-CT guided radiation therapy: technical implementation," *Radiotherapy and Oncology*, vol. 75, pp. 279–286, 2005.

[37] E. Nickoloff, "Current adult and pediatric CT dose," *Pediatr. Radiol*, vol. 32, pp. 250–260, 2002.

[38] A. Palm, E. Nilsson, and L. Herrnsdorf, "Absorbed dose and dose rate using the Varian OBI 1.3 and 1.4 CBCT system," *J. Appl. Clin. Med. Phys*, vol. 11, no. 1, pp. 229–240, 2010.

[39] G. Ding, D. Duggan, and C. Coffey, "Characteristic of kilovoltage x-ray beams used for cone-beam computed tomography in radiation therapy," *Phys. Med. Biol*, vol. 52, pp. 1595–1615, 2007.

[40] "The On-Board Imager Physicist Operations Course," *Varian Medical System, Inc*, 2011.

[41] S. Yoo, G. Kim, R. Hammoud, E. Elder, T. Pawlicki, H. Guan, T. Fox, G. Luxton, F. Yin, and P. Munro, "A quality assurance program for the on-board imager," *Med. Phys*, vol. 33, pp. 4431–4447, 2006.

[42] T. Thorson and T. Prosser, "X-ray volume imaging in image-guided radiotherapy," *Medical Dosimetry*, vol. 31, no. 8, pp. 126–133, 2006.

[43] "XVI R4.5 Application Training Guide, Elekta Limited, 2011.,"

[44] "XVI v 4.5 Clinical User Manual , 2009.,"

[45] N. Mail, D. Moseley, J. Siewerdsen, and D. Jaffray, "The influence of bowtie filtration on cone-beam CT image quality," *Med. Phys*, vol. 36, no. 1, pp. 22–32, 2009.

[46] "TOR 18FG specifications." `http://www.leedstestobjects.com`, 2011.

[47] "OBI 1.5 Customer Acceptance Procedure , 2010.,"

[48] "OsiriX Imaging Software, DICOM Viewer." `http://www.osirix-viewer.com/`, 2003.

[49] "The Phantom Laboratory, Catpan® 504 Manual,"

[50] "The Phantom Laboratory, Catpan® 500 and 600 Manual,"

[51] W. A. Kalender, "Dose in x-ray computed tomography," *Phys. Med. Biol*, vol. 95, pp. R129–R150, 2014.

[52] D. E. Hyer and D. E. Hintenlang, "Estimation of organ doses from kilovoltage cone-beam CT imaging used during radiotherapy patient position verification," *Med. Phys*, vol. 37, no. 9, pp. 4620–4626, 2010.

[53] K. Muralidhar, P. N. Murthy, and R. Kumar, "Commissioning and quality assurance of the x-ray volume imaging system of an image-guided radiotherapy capable linear accelerator," *J. Med. Phys*, vol. 33, no. 2, pp. 72–77, 2008.

[54] "XVI v 4.5 Customer Acceptance Tests , 2009.,"

[55] "XVI R4.5 Instruction for Use , 2009.,"

[56] H. Cheng, V. Wu, E. Liu, and D. Kwong, "Evaluation of radiation dose and image quality for the varian cone beam computed tomography system," *Int. J. Radiation. Oncology. Biol. Phys*, vol. 80, no. 1, pp. 291–300, 2011.

[57] R. Dixon and A. Ballard, "Experimental validation of a versatile system of CT dosimetry using a conventional ion chamber: Beyond $CTDI_{100}$," *Med. Phys*, vol. 34, no. 8, pp. 3399–3413, 2007.

[58] S. Mori, M. Endo, K. Nishizawa, T. Tsunoo, T. Aoyama, H. Fujiwara, and K. Murase, "Enlarged longitudinal dose profiles in cone-beam CT and the need for modified dosimetry," *Med. Phys*, vol. 32, no. 4, pp. 1061–1069, 2005.

[59] "AAPM 2010 Report of AAPM Task Group 111: The future of CT dosimetry: comprehensive methodology for the evaluation of radiation dose in x-ray computed tomography AAPM report no 111," *Am. Assoc. Phys. Med*, 2010.

[60] R. Fahrig, R. Dixon, T. Payne, R. Morin, A. Ganguly, and N. Strobel, "Dose and image quality foe a cone-beam C-arm ct systems," *Med. Phys*, vol. 33, no. 12, pp. 4541–4550, 2006.